JOURNAL OF PETROLOGY | VOLUME 54 | NUMBER 8 | PAGES 1661–1690 | 2013 | doi:10.1093/petrology/egt027

Crystal–Melt Relationships and the Record of Deep Mixing and Crystallization in the AD 1783 Laki Eruption, Iceland

DAVID A. NEAVE[1]*, EMMA PASSMORE[2], JOHN MACLENNAN[1], GODFREY FITTON[3] AND THORVALDUR THORDARSON[3,4]

[1]DEPARTMENT OF EARTH SCIENCES, UNIVERSITY OF CAMBRIDGE, DOWNING STREET, CAMBRIDGE CB2 3EQ, UK

[2]DEPARTMENT OF EARTH SCIENCE AND ENGINEERING, IMPERIAL COLLEGE, LONDON SW7 2AZ, UK

[3]SCHOOL OF GEOSCIENCES, UNIVERSITY OF EDINBURGH, WEST MAINS ROAD, EDINBURGH EH9 3JW, UK

[4]FACULTY OF EARTH SCIENCES, UNIVERSITY OF ICELAND, ASKJA, STURLUGATA 7, 101 REYKJAVIK, ICELAND

RECEIVED SEPTEMBER 4, 2012; ACCEPTED APRIL 5, 2013
ADVANCE ACCESS PUBLICATION MAY 13, 2013

Concurrent mixing and crystallization of magmas has been identified in the plumbing of Icelandic magmatic systems from investigation of their erupted products. Thermobarometric calculations constrain the depth of these processes to the mid- to lower crust. It is currently unknown whether similar processes also occur in the magmas that feed the large fissure eruptions characteristic of the Eastern Volcanic Zone (EVZ). We therefore present the results of an investigation of crystal–melt relationships in the AD 1783 Laki (Skaftár Fires) eruption. The trace element composition of olivine-hosted melt inclusions indicates that concurrent mixing and crystallization of variable mantle melts has occurred in the deep parts of the Laki plumbing system. Magmatic evolution is also recorded in crystal zonation patterns. Zoned plagioclase macrocrysts are made up of three distinct domains: high-anorthite cores, oscillatory zoned mantles and low-anorthite rims. Published mineral–melt equilibrium partition coefficients indicate that macrocryst rims are in equilibrium with the carrier liquid erupted at the surface. High-anorthite cores are more primitive than any other crystal or melt inclusion composition in the magma and are never in equilibrium with melts generated by fractional crystallization models that assume a single liquid line of descent related to the carrier liquid. High-anorthite crystals may have grown from depleted, high-Ca/Na melts of the shallow mantle, which may have been mixed into melts parental to the carrier liquid early in magmatic evolution. The crystal size distribution (CSD) of plagioclase macrocrysts suggests that plagioclase cores represent an assimilated or accumulated crystal population. Cores have acted as nuclei for the growth of oscillatory zoned plagioclase mantles. It is possible to relate the range of plagioclase mantle compositions to the carrier liquid using fractional crystallization models involving eutectic co-crystallization with clinopyroxene and olivine macrocrysts. Negative correlation of titanium and anorthite content in plagioclase mantles confirms that oscillatory zoning is driven by variations in melt composition, most probably the result of repeated recharge and fractionation events. Melt barometry indicates that the melt last equilibrated with olivine, plagioclase and clinopyroxene in the shallow crust at 1–2 kbar, whereas clinopyroxene–melt barometry suggests that the bulk of macrocryst growth occurred within the mid-crust at 2–5·4 kbar. Much of the macrocryst content of the Laki magma occurs as glomerocrysts, of which only rims in contact with the groundmass are in equilibrium with the carrier liquid. This indicates that the formation of glomerocrysts occurred before rim growth, during deposition of crystal mushes in the mid-crust, which subsequently disaggregated upon transport to the shallow crust.

KEY WORDS: *Laki; fractional crystallization; melt inclusions; Iceland; mixing; plagioclase*

INTRODUCTION

It is well known that olivine-hosted melt inclusions from tholeiitic basalts erupted along the rift zones of Iceland have variable trace element compositions (e.g. Gurenko &

*Corresponding author. Telephone: +44 (0)1223 333400. Fax: 01223 333450. E-mail: dan27@cam.ac.uk.

Chaussidon, 1995; Maclennan *et al.*, 2003*b*), which may interpreted as a record of concurrent mixing and crystallization of diverse mantle melts (Maclennan, 2008*a*). Recent work has also demonstrated that the crystal load of magmas can preserve a history of growth from primitive melts of different composition (Winpenny & Maclennan, 2011). Thermobarometry has constrained the depth of the processing of primitive melts in Iceland to the mid- to lower crust (e.g. Winpenny & Maclennan, 2011). Previous studies of mixing of variable mantle melts have focused on the Northern Volcanic Zone (Maclennan *et al.*, 2003*a*), Western Volcanic Zone and Reykjanes Peninsula (Gurenko & Chaussidon, 1995; Maclennan 2008*a*, 2008*b*). Only the recent study of Moune *et al.* (2012) on Fimmvörðuháls–Eyjafjallajökull has commented on a potential melt inclusion record of variable mantle melts in the Eastern Volcanic Zone (EVZ) of Iceland. We investigate whether processes similar to those operating in the plumbing systems of smaller eruptions are recorded in the large basaltic fissure eruptions that characterize volcanism in the EVZ, with the AD 1783 Laki eruption being the focus of this study.

The observation of deep seismicity associated with the 2010 eruption of Eyjafjallajökull has provided evidence for continuing melt storage and transport in the lower to mid-crust under the EVZ (Hjaltadóttir *et al.*, 2009; Sigmundsson *et al.*, 2010; Tarasewicz *et al.*, 2012). By studying the petrology of eruptions in the EVZ it may be possible to improve the understanding of the nature and causes of such geophysical phenomena, as well as associated geodetic signals. However, before undertaking thermobarometric work on the Laki magma, it is important to understand the deep processes that have controlled its evolution.

The relationships between crystals and the melts in which they are carried provide crucial information about the processes that occur prior to eruptions. Genetic relationships between melt and crystals have traditionally been considered in terms of two end-members: phenocrysts, which are in equilibrium with their host melt [e.g. Cox *et al.* (1979) referred to phenocrysts as the solid phases in equilibrium with a liquid prior to quenching], and xenocrysts, which have been assimilated into a melt different from that in which they crystallized (e.g. Harker, 1896). However, observations often indicate that relationships between crystals and melt are more complex than can be described using simple end-member terms. Such observations have led to the development of the term antecryst to describe crystals that are from the same magmatic system, but are out of equilibrium with their host melt (after W. Hildreth at the 'Longevity and Dynamics of Rhyolitic Magma Systems', Penrose Conference, 2001; Davidson *et al.*, 2007). However, it is often difficult to define discrete magmatic systems, especially in the presence of a wide range of primary melts. This limits the use of the term antecryst in this context. To avoid preconceptions imposed by genetic terminology in this study, we have used non-genetic terminology based on the description of kimberlites following the rationale of Thomson & Maclennan (2013). Crystals that are larger than the groundmass and within the size interval ~0·2–10 mm are referred to as macrocrysts (Skinner & Clement, 1979).

To understand crystal–melt relationships, a range of microanalytical, imaging and textural techniques must be used to disentangle the history of a magmatic system. The compositional variability of melt inclusions has been demonstrated to exceed the variability in the erupted melt in a number of magmatic systems (e.g. Sobolev & Shimizu, 1993; Saal *et al.*, 1998; Maclennan, 2008*a*). Indeed, the generation of diverse primary melts is predicted from fractional melting models (e.g. Gast, 1968; Kelemen *et al.*, 1997). We investigate whether mantle melt diversity is recorded in melt inclusions in the EVZ, at Laki, as it is elsewhere in Iceland (e.g. Gurenko & Chaussidon, 1995; Slater *et al.*, 2001; Maclennan, 2008*b*). If diverse melts are supplied to the system it is expected that these will undergo concurrent mixing and crystallization as they cool. If mixing of tracers unaffected by crystallization processes approaches completion the erupted melt will represent the mean composition of all melts supplied to the system. A decrease of melt variability with crystallization is well characterized in melt inclusion studies (Maclennan, 2008*a*). A study of clinopyroxenes from Borgarhraun, in the Northern Volcanic Zone of Iceland, demonstrates that macrocrysts are also capable of preserving a record of mantle melt variability (Winpenny & Maclennan, 2011). The association of high-Mg# clinopyroxene with depleted melt compositions highlights a key consequence of the generation of magmas from diverse primitive melts: magmatic evolution will not follow a single liquid line of descent. Prior to mixing, variable primitive melts will evolve along different liquid lines of descent and will be in equilibrium with different crystal phases of different composition. Consequently, modelling approaches that are reliant on following single liquid lines of descent may be unable to reproduce the observed melt and crystal compositions. We therefore consider the role of melt variability in controlling macrocryst diversity when investigating the composition of Laki macrocrysts.

Some phyric magmas in Iceland are thought to carry disaggregated crystal mushes; for example, the tuff cones Brandur, Fontur and Saxi (Hansen & Grönvold, 2000; Holness *et al.*, 2007), the table mountains Miðfell and Mælifell (Gurenko & Sobolev, 2006), and Laki itself (Passmore *et al.*, 2012). These mushes may be cognate with the eventual carrier liquid, or form from melts that are closely related but distinct. For example, isotopic disequilibrium between plagioclase macrocrysts and the carrier

liquid in both the 8600 BP Thjórsárhraun lava and its hypothesized source vents at Fontur and Saxi has been used to argue that the macrocrysts and the carrier liquid are not cogenetic (Halldorsson *et al.*, 2008). When undertaking thermobarometry dependent on crystal compositions, it is important to consider whether crystals are cogenetic or are entrained from a mush, so that pressures can be assigned to processes in the appropriate component of the magmatic system.

The AD 1783 Laki eruption is the largest basaltic fissure eruption in Iceland to have been observed directly (Thordarson *et al.*, 1996) and provides an ideal case for studying deep processes in such eruptions because it has been widely sampled and studied, providing good context for this work.

Geological setting

The Lakagígar cone row, along which the AD 1783 Laki eruption took place, is located within the Grímsvötn volcanic system in the Eastern Volcanic Zone (EVZ) of Iceland (Thordarson & Self, 1993; Fig. 1). The EVZ is the most magmatically productive of the neovolcanic zones in Iceland, accounting for 79% of the magma volume erupted in Iceland since settlement in AD 874, with Grímsvötn having erupted at least 70 times over this period (Larsen, 2000; Thordarson & Larsen, 2007). Global positioning system (GPS) studies indicate that spreading rates vary along the EVZ, with faster spreading in the north than in the south (LaFemina *et al.*, 2005; Geirsson *et al.*, 2006), where the rift is propagating southwestwards under the Vestmannaeyjar (Steinthorsson *et al.*, 1985). The geochemistry of erupted products reflects this variability in spreading rate, as well as the maturity of the fissure swarm (Thordarson & Larsen, 2007). Laki is located in the faster spreading northern portion of the EVZ where tholeiitic basalts are erupted. Alkali basalts are erupted in the slower spreading southern portion (Jakobsson, 1979). Volcanism in the EVZ is characterized by large fissure eruptions. The $\sim$19·1 km^3 dense rock equivalent (DRE) AD 934–938 Eldgjá eruption in the Katla system and the 15·1 km^3 DRE AD 1783–1784 Laki eruption (Thordarson & Larsen, 2007) are the largest volume fissure eruptions from historical time in Iceland.

The Laki eruption

Thordarson & Self (1993) have provided a detailed description of the physical volcanology and timeline of the Laki eruption, known locally as the Skaftáreldar (Skaftár Fires). The eruption took place over approximately 8 months, from June 1783 to February 1784, as part of a 2 year long volcano-tectonic episode in the Grímsvötn volcanic system along a 27 km long series of 10 en echelon fissures that opened in a step-wise fashion from SW to NE. Opening of each fissure is considered as a distinct phase of eruption and was characterized by a short-lived explosive phase, which gave way to weaker fountaining activity and lava effusion. Fissures I–V opened to the SW of Laki Mountain, from which the eruption gets its name, and fissures VI–X to the NE. During phases I–V lava was channelled from its source in the highlands down the Skaftá river gorge onto the Síða coastal plain (Fig. 1). During phases VI–X lava was largely channelled down the Hverfisfljót river gorge. The lava eventually covered an area of $\sim$600 km^2. Detailed studies of shallow degassing and lava flow emplacement have been undertaken by Thordarson *et al.* (1996) and Guilbaud *et al.* (2007).

Sigmarsson *et al.* (1991) reported that the lava erupted throughout all phases was quartz-normative and showed a high degree of isotopic homogeneity. Passmore *et al.* (2012), however, observed statistically significant variations in both whole-rock and crystal compositions from samples collected across the Laki system. Whole-rock variations were interpreted as a signal of variable degrees of mush addition shortly prior to eruption at shallow depths. Passmore *et al.* (2012) also observed that variability in crystal composition correlates with eruption phase, with later phases erupting more primitive mean compositions (higher Mg# clinopyroxene, more anorthitic plagioclase and more forsteritic olivine). Previous melt inclusion studies of Laki have focused on volatiles and hence the gas output of the eruption (Métrich *et al.*, 1991; Thordarson *et al.*, 1996). However, the new melt inclusion data presented here are focused on investigating deep magmatic processes.

SAMPLE COLLECTION

Samples were selected from a set of 47 basalt hand specimens and seven tephra samples collected by E. Passmore and co-workers (Passmore *et al.*, 2012). Sample locations are shown in Fig. 1. Lava and tephra samples were collected between 2004 and 2006 from distal and proximal regions of flows across a range of eruption phases. Details of sampling strategy have been discussed by Passmore *et al.* (2012) and details of sample locations are included in Supplementary Data Electronic Appendix 1 (available for downloading at http://www.petrology.oxfordjournals.org).

METHODS

Microscopy

Samples were analysed optically using a petrographic microscope. Backscattered electron (BSE) images were produced from thin sections using a JEOL JSM-820 scanning electron microscope (SEM) in the Department of Earth Sciences at the University of Cambridge, UK. An accelerating voltage of 15 kV was used with a working distance of 16 mm. Cathodoluminescence (CL) images were produced using a Gatan MonoCL instrument interfaced with the SEM.

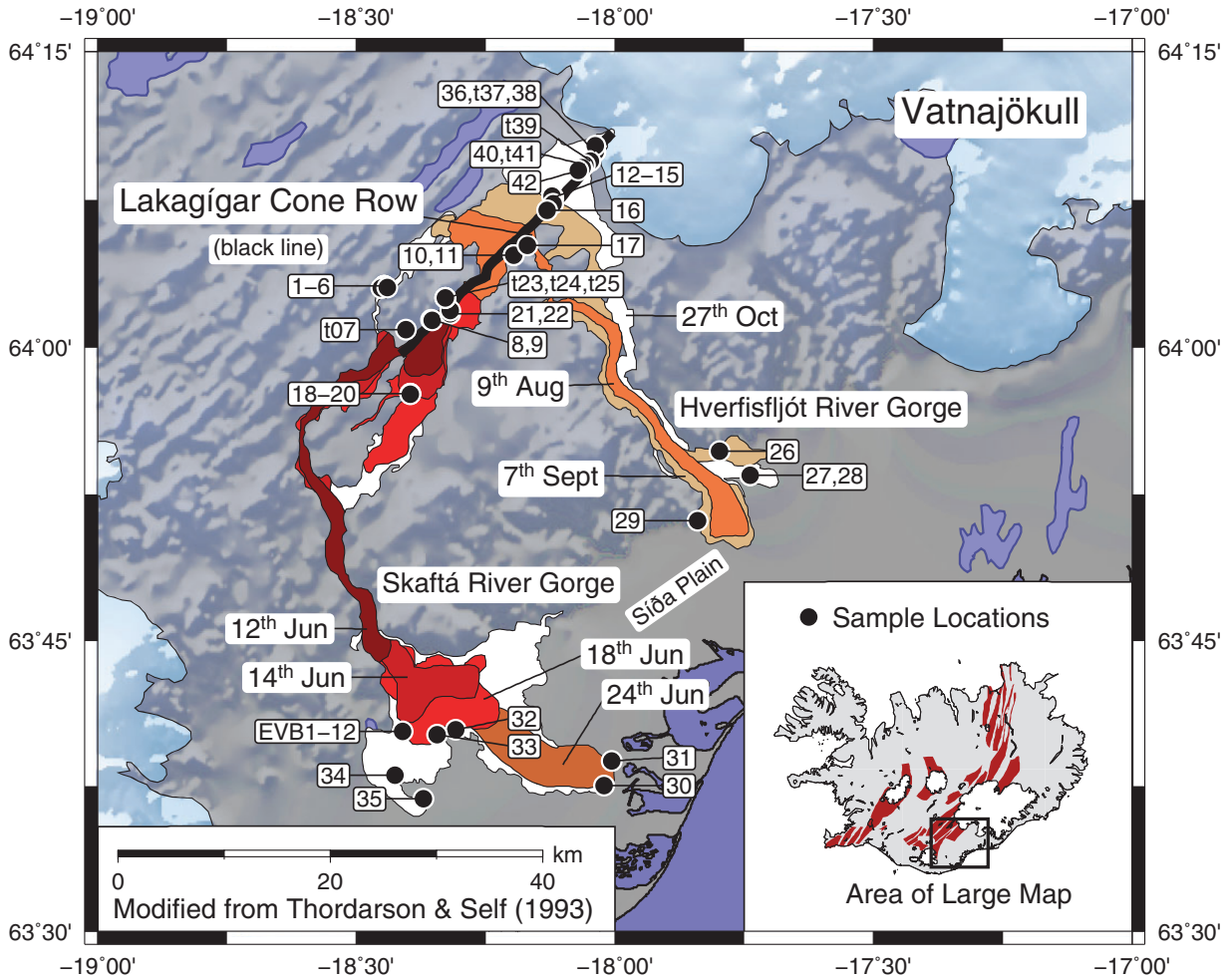

Fig. 1. Map showing the extent of flows emplaced during the AD 1783 Laki eruption. The 27 km long series of fissures is shown as a thick NE–SW-striking black line. The earliest eruptions were in the SW and moved through time to the NE. Dates of lava lobe emplacement illustrate how the lava flowed from source vents down gorges to the coastal plain. Black circles and associated sample numbers show the location of the samples collected by Passmore *et al.* (2012) that were used in this study. The inset map in the bottom right shows the location of the Laki fissure within the Eastern Volcanic Zone (EVZ) in south Iceland. Flow boundaries and dates are reproduced from Thordarson & Self (1993).

Electron microprobe analysis

Major element compositions of crystals were determined by electron microprobe analysis (EMPA) using a Cameca SX100 electron microprobe in the Department of Earth Sciences at the University of Cambridge, UK. A focused beam with an operating potential of 15 kV and a beam current of 10 nA for major elements and 100 nA for minor elements was used for crystal analyses. Peak counting times were as follows: 20 s for major elements, 30 s for trace elements, apart from Ti, which was counted for 60 s in plagioclase, and Na, which was counted for 10 s. Standards used were jadeite for Na, periclase for Mg, fused Si for Si, K-feldspar for K, rutile for Ti, fayalite for Fe, corundum for Al, apatite for P, and pure metals for Cr, Mn and Ni. Most analyses returned totals of 98·5–100·5 wt %. Samples with totals outside this range were discarded in subsequent analysis as were samples with erroneous stoichiometry; for example, clinopyroxenes with >4·1 and <3·9 cations calculated on the basis of six oxygens.

Crystal compositions are summarized throughout in terms of anorthite content for plagioclase [An = 100 × atomic Ca/(Ca + Na)], magnesium number for clinopyroxene [Mg# = 100 × atomic Mg/(Mg + Fe)] and forsterite content for olivine [Fo = 100 × atomic Mg/(Mg + Fe)]. Repeat analyses of standards were used to estimate the precision of An, Mg# and Fo measurements. Anorthite content in the Anorthite55 standard was determined with a precision of $2\sigma = 1{\cdot}00$ mol % ($n = 40$). Forsterite content of the St. John's Island Olivine standard was determined with a precision of $2\sigma = 0{\cdot}46$ mol % ($n = 27$). Precision of Mg# of clinopyroxene was similar to the precision of forsterite content in olivine.

Major element compositions of glasses were determined by EMPA using a Cameca SX100 electron microprobe in the School of GeoSciences at the University of Edinburgh, UK. An 8 μm beam with an operating potential of 15 kV and a beam current of 10 nA were used. Peak counting times were as follows: 10 s for major elements and 30 s for trace elements. Most analyses returned totals of 97–100·5 wt %. Totals outside this range were discarded in subsequent analysis.

Melt inclusion preparation

A subset of 12 of the 54 samples that contained sufficient olivine macrocrysts were crushed at the School of GeoSciences in Edinburgh to pick grains for melt inclusion analysis. Most inclusions experienced post-entrapment crystallization and required re-homogenization before analysis. Olivine crystals were heated to 1220°C for 20 min in Pt capsules in a 1 atm gas-mixing furnace at fO_2 ~2 log units below the quartz–fayalite–magnetite (QFM) buffer to prevent oxidation. fO_2 was maintained with a controlled gas-mix of either H_2–CO_2 or CO–CO_2.

Secondary ion mass spectrometry

A total of 131 melt inclusions were analysed by secondary ion mass spectrometry (SIMS) for selected trace elements and rare earth elements (REE) at the NERC Ion Microprobe Facility in the School of GeoSciences at the University of Edinburgh, UK on a Cameca IMS-4f instrument. Care was taken to select melt inclusions only in uncracked crystals that were not connected to the carrier melt by melt channels. A non-rastered <20 μm diameter primary beam of O^- ions with an operating potential of 15 kV and a beam current of 5 nA was used throughout. The following isotopes were analysed by counting for 3 s in each cycle of a six cycle run: ^{26}Mg, ^{30}Si, ^{42}Ca, ^{47}Ti, ^{85}Rb, ^{88}Sr, ^{89}Y, ^{90}Zr, ^{93}Nb, ^{138}Ba, ^{139}La, ^{140}Ce, ^{141}Pr, ^{143}Nd, ^{149}Sm, ^{151}Eu, ^{157}Gd, ^{159}Tb, ^{161}Dy, ^{165}Ho, ^{167}Er, ^{169}Tm, ^{171}Yb and ^{175}Lu. Absolute element concentrations were calculated using JCION-5 software by normalizing intensities to ^{30}Si, which had been determined externally by EMPA. Peak positions were verified before each analysis, and mass 130·5 was measured as background for 5 s in each cycle and was always sufficiently close to zero to be ignored. Corrections were made for oxide interferences of light REE (LREE) on the heavy REE (HREE) and BaO on Eu. The magnitude of the correction was measured on synthetic REE-bearing glasses under the same analytical conditions and then applied to the data. Oxide interferences were monitored by the addition of ^{154}BaO/Ba and ^{156}CeO/Ce in each analysis; these ratios showed little variation throughout the analytical period. Ion yields determined by analysis of the NIST SRM610 standard (e.g. Jochum *et al.*, 2011) showed no systematic drift through the course of the analyses. An average ion yield calculated at the end of the analyses was used to calibrate the melt inclusion data.

BSE image calibration

The intensity of a BSE image directly correlates with the density of the material being imaged (Reed, 2005). In plagioclase there is a linear relationship between anorthite content and density, and hence with BSE intensity (Ginibre *et al.*, 2002*a*). In a thin section of sample LAK12 the correlation between anorthite and BSE intensity was tested and found to be strong ($r^2 = 0{\cdot}83$). If BSE images are coincident with EMPA analyses, then BSE image grayscale was calibrated for anorthite content using EMPA data and the image processing tool ImageJ (Abràmoff *et al.*, 2004).

Crystal size distribution (CSD) calculation

Data for CSD calculations were extracted from stitched and edited BSE images using the 'analyse particles' tool in ImageJ. The Microsoft Excel spreadsheet CSDslice (Morgan & Jerram, 2006) was used to calculate a best-fit crystal habit of 9:3:1 (length:width:depth) for Laki plagioclase to perform stereological conversion and CSD calculations with CSDCorrections (Higgins, 2000).

RESULTS

Petrography

The Laki lava is porphyritic and contains three macrocryst phases throughout: olivine, clinopyroxene and plagioclase (Fig. 2). Macrocrysts are present either as single grains or in glomerocrysts, which may be mono- or poly-mineralic. Macrocrysts of both types have the same size ranges. Plagioclase is typically 150–2000 μm, with a minor population in the range 2–8 mm, and clinopyroxene and olivine are commonly 200–1000 μm, with a rare clinopyroxene subpopulation in the range 1–8 mm. Point counting indicates that, on average, macrocrysts make up 12% of the Laki lava by mass in the ratio 57:11:32 plg:ol:cpx (Passmore *et al.*, 2012). Some Fe–Ti oxides are present but these are restricted to small groundmass grains in the more crystalline samples and are never observed as inclusions within phenocrysts. No significant sulphides have been observed in the groundmass.

Most plagioclase is present as tabular grains in glomerocrysts, which is consistent with the observations of Guilbaud *et al.* (2007). Macrocrysts are largely sub- to euhedral, whereas groundmass grains are sub- to anhedral and often display swallowtail morphology (Guilbaud *et al.*, 2007). Clinopyroxene macrocrysts are generally prismatic and sub- to euhedral and often contain numerous plagioclase inclusions. Olivine macrocrysts are generally oval and subhedral.

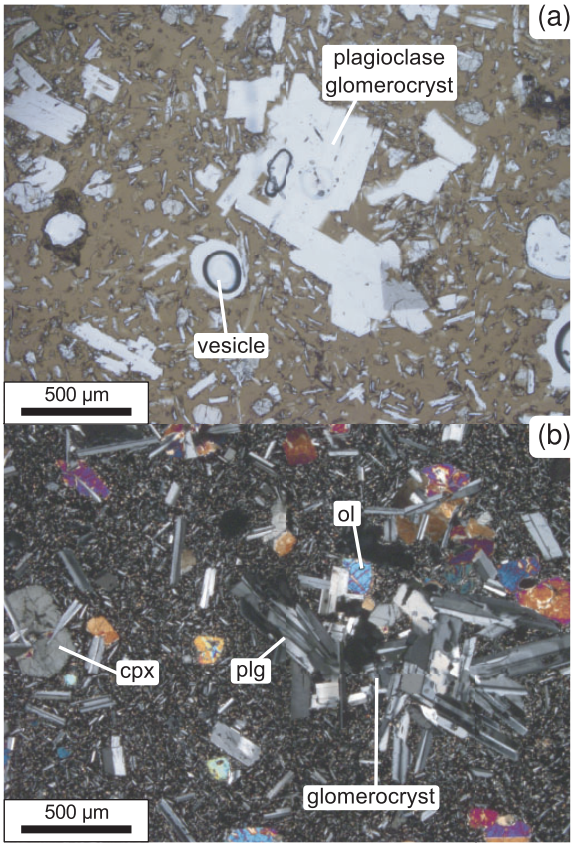

Fig. 2. Photomicrographs showing typical Laki lava samples. (a) Photomicrograph with plane polars of sample LAK04. The plagioclase-rich glomerocryst in the centre of the field of view should be noted. Plagioclase, clinopyroxene and olivine phenocrysts are all observed scattered in the glassy groundmass. Smaller groundmass grains of all three phases are also visible. The absence of opaque Fe–Ti oxides should be noted. (b) Photomicrograph with crossed polars of sample LAK12. Polymineralic glomerocrysts containing plagioclase, clinopyroxene and highly birefringent olivine are set in a finely crystalline groundmass composed of plagioclase, clinopyroxene and olivine.

Major and trace element compositions of crystals

Plagioclase macrocryst compositions measured in this study and by Passmore *et al.* (2012) lie in the range $An_{53–89}$. The composition of plagioclase groundmass grains lies in the range $An_{51–64}$. Clinopyroxene macrocryst compositions lie in the range Mg# 50–83. Clinopyroxene groundmass grain compositions are Mg# ~65–75, although few analyses of groundmass grains are available, in contrast with plagioclase. Olivine macrocryst compositions measured by Passmore *et al.* (2012) in the same samples have compositions that lie in the range $Fo_{60–86}$. Olivine groundmass grain compositions, again measured by Passmore *et al.* (2012), are $Fo_{52–72}$. Typical major element compositions of the macrocryst phases are presented in Table 1. The ranges of mineral compositions are summarized in Fig. 3, along with the crystal compositions predicted to be in equilibrium with the average tephra glass composition of Passmore *et al.* (2012) (see Table 1), using a fixed Kd^{ol-liq}_{Mg-Fe} of 0·3 (Roeder & Emslie, 1970) for olivine, a Kd^{ol-liq}_{Mg-Fe} determined using the model of Wood & Blundy (1997) for clinopyroxene, and the model of Namur *et al.* (2011) for the anorthite content of plagioclase. The magmatic system was assumed to have an oxygen fugacity of 1 log unit below the QFM buffer, which corresponds to an $Fe^{3+}/\Sigma Fe$ ratio of ~0·1 in Icelandic basalts (Maclennan, 2008*a*). This represents a good approximation because $Fe^{3+}/\Sigma Fe$ measured in Icelandic systems lies within a relatively confined range of 0·08 (Breddam, 2002) to 0·132 (Óskarsson *et al.*, 1994).

A large number of rim and groundmass compositions are much more evolved than the crystal compositions calculated to be in equilibrium with tephra glass compositions. Crystal–melt equilibrium model uncertainties may explain some of this discrepancy. However, most of these evolved compositions are likely to be the result of large extents of syn-eruptive crystallization as magma is emerging from vents and forming lava flows (Guilbaud *et al.*, 2007). New crystal composition data are summarized in plots of anorthite content vs TiO_2, FeO_t and MgO and clinopyroxene Mg# vs TiO_2 in Fig. 4. The full dataset is available in Supplementary Data Electronic Appendix 2.

Olivine and olivine-hosted melt inclusions

The crystal load of the Laki magma is generally much more primitive than that predicted to be in equilibrium with the carrier liquid (Passmore *et al.*, 2012; Fig. 3). These primitive crystals may therefore contain information about pre-eruptive, deep processes. Melt inclusions trapped in primitive crystals during the course of melt evolution have become widely employed in petrogenetic studies. For example, large variations in the REE content of Icelandic olivine-hosted melt inclusions have been observed by various researchers (Gurenko & Chaussidon, 1995; Slater *et al.*, 2001; Maclennan *et al.*, 2003*a*, 2003*b*; Maclennan, 2008*a*; Moune *et al.*, 2012). Maclennan *et al.* (2003*a*) demonstrated that olivine-hosted melt inclusions from Borgarhraun in North Iceland record a history of concurrent mixing and crystallization.

Olivine compositions from Laki macrocrysts range across a long crystallization interval from Fo_{68} to Fo_{86}. Melt inclusions trapped in these olivines provide an ideal target for investigation of magmatic evolution. However, the major element composition of melt inclusions is highly affected by post-entrapment processes (e.g. Danyushevsky *et al.*, 2002). Equilibrium olivine forsterite contents of melt inclusions calculated using a constant Kd^{ol-liq}_{Mg-Fe} of 0·3 (Roeder & Emslie, 1970) underestimate the measured forsterite composition of the host by 4–10 mol % for naturally quenched inclusions and overestimate by 3–9 mol % for re-homogenized inclusions. Melt inclusion Mg# is therefore not representative of original trapped values.

Table 1: Typical compositions of macrocrysts from the Laki lava determined by EMPA

Sample:	LAK06	LAK06	LAK17	LAK03	LAK26	LAK04	LAK06	Mean
Phase:	Plagioclase	Plagioclase	Plagioclase	Clinopyroxene	Clinopyroxene	Olivine*	Olivine*	Tephra
Context:	Macrocryst core	Macrocryst mantle	Macrocryst rim	Macrocryst core	Macrocryst rim	Macrocryst core	Macrocryst rim	Glass*
SiO_2 (wt %)	46·17	48·81	52·42	50·89	49·95	39·06	35·54	48·95
TiO_2	0·02	0·06	0·11	0·85	1·32	0·00	0·03	3·11
Al_2O_3	33·86	31·59	29·28	3·40	2·55	0·05	0·06	12·81
FeO_t	0·50	0·71	0·92	6·11	11·85	15·71	30·01	14·23
MnO	n.m.	n.m.	n.m.	0·15	0·29	0·26	0·41	0·25
MgO	0·10	0·14	0·17	16·19	14·64	43·96	32·68	5·54
CaO	17·52	15·80	12·75	20·71	17·79	0·31	0·38	9·63
Na_2O	1·51	2·66	4·27	0·26	0·27	0·01	0·03	2·74
K_2O	0·03	0·07	0·09	0·00	0·00	n.m.	n.m.	0·46
P_2O_5	n.m.	n.m.	n.m.	n.m.	n.m.	n.m.	n.m.	0·43
NiO	n.m.	n.m.	n.m.	0·02	0·01	n.m.	n.m.	n.m.
Cr_2O_3	n.m.	n.m.	n.m.	0·67	0·05	0·05	0·03	n.m.
An (mol %)	86·54	76·76	62·24					
Mg#				82·52	68·77			
Fo (mol %)						83·30	66·00	
Total	99·71	99·82	100·02	99·27	98·72	99·58	99·19	

*Data and the mean tephra glass composition from Passmore *et al.* (2012).
n.m., not measured.

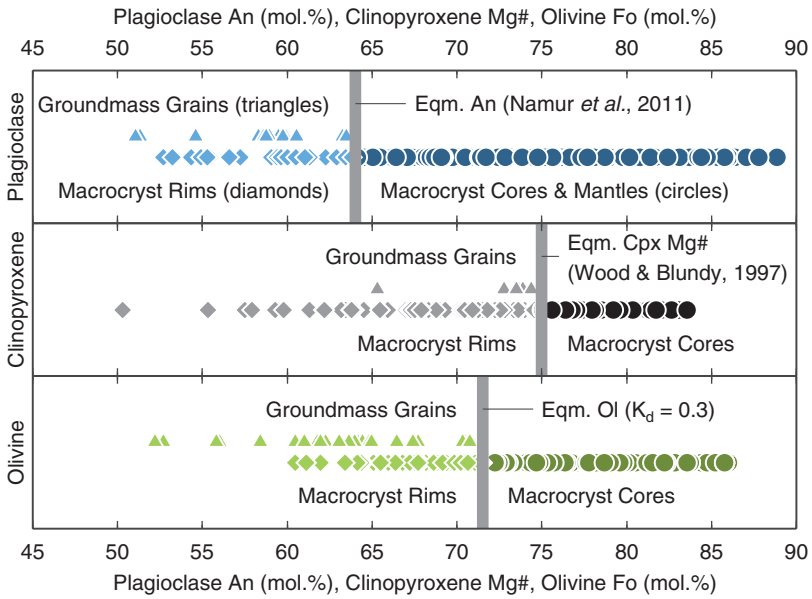

Fig. 3. Summary of crystal composition ranges determined by EMPA. Olivine data are from Passmore *et al.* (2012). The vertical bars represent melt macrocryst compositions in equilibrium with the average tephra glass composition of Passmore *et al.* (2012) (Table 1) calculated using the model of Namur *et al.*, (2011) for plagioclase, the model of Wood & Blundy (1997) for clinopyroxene and a constant $K_d^{ol-liq}_{Mg-Fe}$ of 0·3 for olivine. Macrocryst cores and mantles (circles) are more primitive than the composition calculated to be in equilibrium with the erupted melt, whereas rims (diamonds) and groundmass grains (triangles) are more evolved.

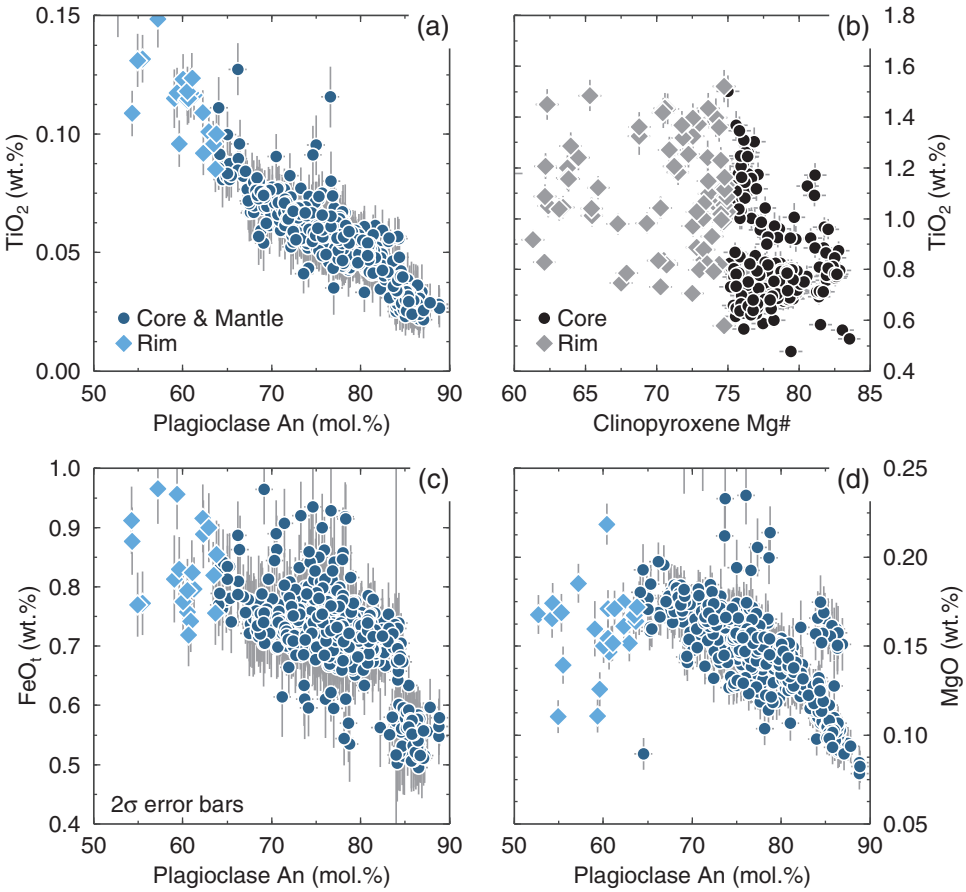

Fig. 4. Plots summarizing crystal composition data collected by EMPA in this study. (a) Plagioclase anorthite (mol %) [An = 100 × atomic Ca/(Ca + Na)] vs TiO_2 (wt %). (b) Clinopyroxene Mg# [Mg# = 100 × atomic Mg/(Mg + Fe)] vs TiO_2 (wt %). (c) Plagioclase anorthite mol % vs FeO_t (wt %). (d) Plagioclase anorthite mol % vs MgO (wt %). Detection limit for MgO during EMPA was lower than 0·05 wt %. The 2σ errors are shown.

Although the concentration of CaO and Na_2O in olivine-hosted melt inclusions will be affected by the removal or addition of olivine at inclusion walls, Ca/Na (expressed throughout as an atomic ratio) of inclusions will remain stable because both elements are incompatible in olivine ($D_{Ca}^{ol-melt} = 1{\cdot}25 \times 10^{-2}$, $D_{Na}^{ol-melt} = 8\text{–}47 \times 10^{-3}$ at 1300°C in San Carlos olivine; Spandler & O'Neill, 2010). The rate of diffusion of Ca or Na in olivine is comparable with, or slower than, the rate of Fe–Mg inter-diffusion (Jurewicz & Watson, 1988; Spandler & O'Neill, 2010). Therefore if the forsterite content of an olivine reliably represents the composition of the melt from which it grew, then the Ca/Na of melt inclusions in the olivine will be representative of the original trapped melt compositions. All Laki melt inclusions, whether naturally quenched or re-homogenized, have Ca/Na < 4 (Fig. 5a). The complete major and trace element data are reported in Supplementary Data Electronic Appendix 3.

Both homogenized and naturally quenched melt inclusions exhibit overlapping ranges of trace element compositions (e.g. Fig. 5b). Trace element ratios in melt inclusions are therefore not greatly affected by the homogenization process. The average REE profile of melt inclusions is similar in form to the average whole-rock REE profile. REE profiles for the lowest and highest La/Yb inclusions are plotted in Fig. 5c to illustrate that single melt inclusions have profiles of different steepness. This variable steepness of REE profiles is expressed as different La/Yb values in Fig. 5b. The range in melt inclusion La/Yb is greatest in the most forsteritic ($Fo_{>83}$) olivines and decreases with decreasing forsterite content. Melt inclusions hosted in $Fo_{<76}$ olivines have concentrations that are closest to equilibrium with the carrier liquid (Fig. 5b).

To statistically validate the decrease of La/Yb variation with forsterite content, the data were split into three populations: $Fo_{>83}$ olivines, which have been previously described as xenocrysts by some researchers (Bindeman *et al.*, 2006; Guilbaud *et al.*, 2007), $Fo_{<76}$ olivines, which are most similar to predicted whole-rock equilibrium compositions, and $Fo_{76–83}$ olivines, which lie between the other two populations. The standard deviation of La/Yb in $Fo_{>83}$-hosted melt inclusions is 0·64 ($n = 57$), in $Fo_{76–83}$-hosted melt

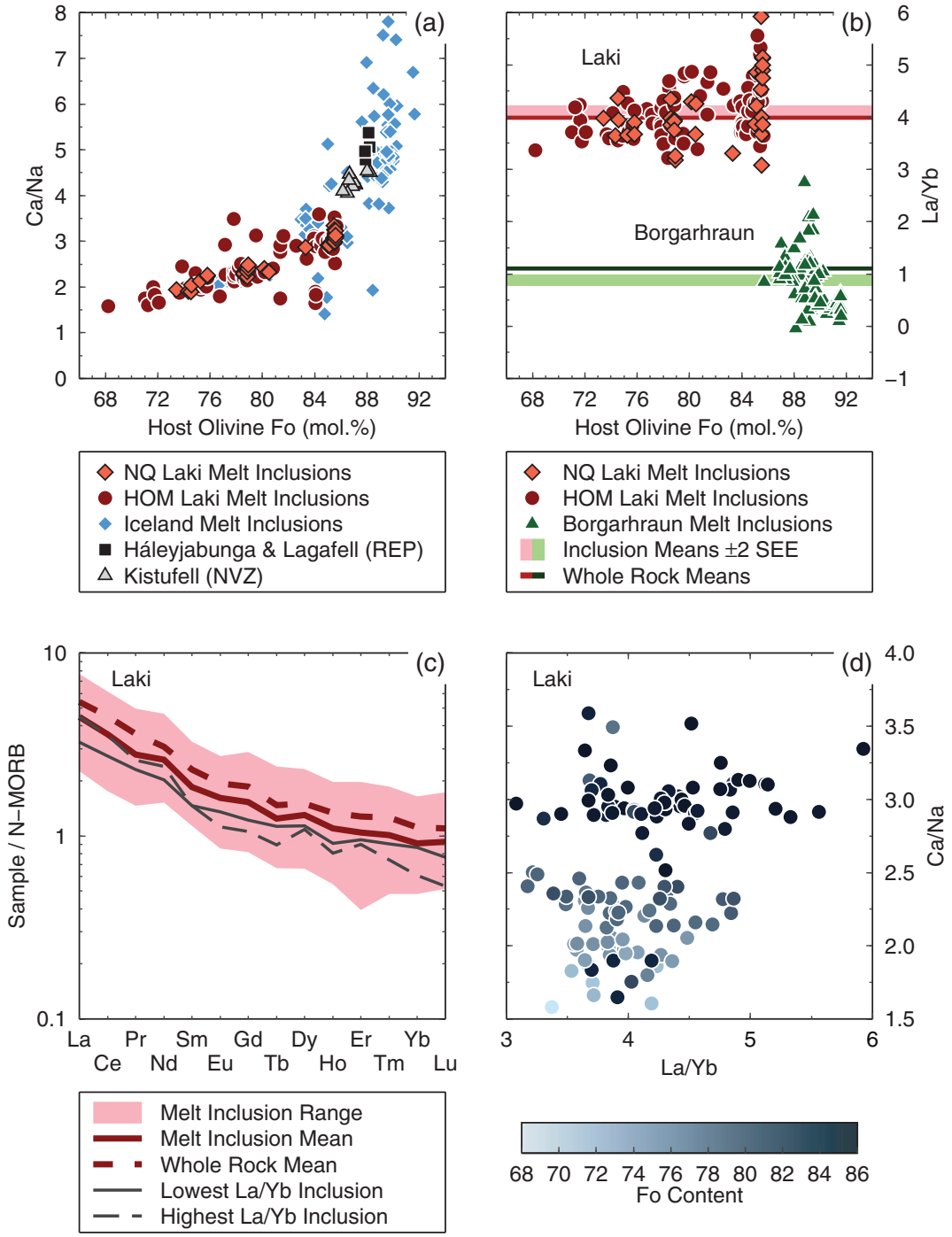

Fig. 5. Melt inclusion composition data. (a) Ca/Na in melt inclusions plotted against forsterite content of their host olivines. Laki melt inclusions all lie at low Ca/Na values, whereas values from a compilation of Icelandic melt inclusions reach much higher values. Re-homogenized (HOM) melt inclusions from Laki are shown as dark circles and naturally quenched (NQ) inclusions as pale diamonds. Data collated from Gurenko & Chaussidon (1995, 1997, 2002), Slater *et al.* (2001), Maclennan *et al.* (2003*a*, 2003*b*) and Maclennan (2008*a*, 2008*b*). Matrix glass compositions of eruptions containing (near) equilibrium high-anorthite plagioclase from Háleyjabunga and Lagafell (Gurenko & Chaussidon, 1995) and Kistufell (Breddam, 2002) are included for comparison. (b) Host olivine forsterite plotted against La/Yb for both Laki melt inclusion data and Borgarhraun data (Maclennan *et al.*, 2003*b*). Re-homogenized (HOM) melt inclusions from Laki are shown as dark circles and naturally quenched (NQ) inclusions as diamonds. (c) Normal (N)-MORB-normalized REE diagram showing that all melt inclusions have similar REE patterns to the mean whole-rock pattern, which is similar to the mean melt inclusion pattern. The profiles of the highest and lowest La/Yb inclusions are also shown. (d) Melt inclusion Ca/Na plotted against La/Yb. Points are shaded by forsterite content with pale shading for low forsterite, down to Fo_{68}, and dark for high forsterite up to Fo_{86}. Ca/Na does not vary with La/Yb at constant forsterite content. Ca/Na decreases with forsterite content of the host olivine.

inclusions it is 0·46 ($n = 40$) and in $Fo_{<76}$-hosted melt inclusions it is 0·27 ($n = 31$). Upper and lower confidence intervals of the standard deviation were calculated using the chi-squared distribution at 69% (1σ) and 95% (2σ) confidence levels. At the 69% confidence level confidence intervals do not overlap ($Fo_{>83} = 0{\cdot}58$–$0{\cdot}71$; $Fo_{76–83} = 0{\cdot}41$–$0{\cdot}52$; $Fo_{<76} = 0{\cdot}24$–$0{\cdot}31$). At the 95% confidence level there is only minor overlap between the two more forsteritic populations ($Fo_{>83} = 0{\cdot}54$–$0{\cdot}79$; $Fo_{76–83} = 0{\cdot}38$–$0{\cdot}59$; $Fo_{<76} = 0{\cdot}21$–$0{\cdot}36$). The decrease in melt inclusion La/Yb variance with host olivine forsterite content is therefore a statistically significant feature of the eruption.

Plagioclase zonation

Plagioclase macrocrysts exhibit complicated internal compositional structures. Grains display three distinct compositional domains, which are marked in Fig. 6. Many large grains contain a homogeneous, high-anorthite core of $An_{84–89}$, wrapped by an $An_{70–84}$ mantle that is oscillatory zoned. The oscillatory zoning has a wavelength that is too short to be clearly resolved on EMPA profiles. Where no high-anorthite cores are present the centres of macrocrysts are composed of oscillatory zoned $An_{70–84}$ plagioclase. Macrocryst rims have anorthite contents that decrease outwards from An_{70} to An_{54}. Only the outermost rim values are comparable with groundmass grains. The rims wrap around joined macrocrysts. The presence of sharp changes in anorthite content on EMPA profiles (Fig. 6) is consistent with the slow rate of NaSi–CaAl inter-diffusion ($D = 1 \times 10^{-21}$ to $1 \times 10^{-22}\,m^2\,s^{-1}$ in $An_{70–90}$ at 1150°C; Grove *et al.*, 1984).

Zoning is also observed in the trace element content of plagioclase. TiO_2 shows a strong negative correlation with anorthite, with low values of 0·025 wt % in crystal cores and much larger values of 0·125 wt % in crystal rims, which are comparable with TiO_2 concentrations in groundmass grains of ~0·13 wt % (Fig. 4a). These concentrations are comfortably above the 0·007 wt % EMPA detection limit for TiO_2. The absence of Fe–Ti oxide as a macrocryst phase in the Laki lava indicates that oxide saturation was not reached during crystal growth in the subsurface. The only Fe–Ti oxides present are small dendritic grains that grew during groundmass crystallization. Titanium therefore behaved incompatibly during the evolution of the Laki magma [At 1200°C the following partition coefficients are calculated using the models of Bindeman & Davis (2000), Wood & Blundy (1997) and Bédard (2005) respectively: $D_{Ti}^{plg-melt}$ ~0·04; $D_{Ti}^{cpx-melt}$ ~0·4; $D_{Ti}^{ol-melt}$ ~0·04]. Titanium is also likely to have a very slow rate of diffusion in plagioclase because of its large charge and hence is a reliable tracer of magmatic evolution (Humphreys, 2009).

FeO_t shows a weak negative correlation with anorthite, but is somewhat scattered (Fig. 4c). Notably high-anorthite cores record FeO_t compositions ~0·15 wt % lower than oscillatory zoned mantles. Fe diffusion must occur at a sufficiently slow rate to preserve a step change in FeO_t at An_{84} boundaries within macrocrysts. The FeO_t–An negative correlation is therefore likely to be a magmatic signal rather than the result of diffusive equilibration.

MgO shows a more complicated relationship with anorthite, negatively correlating at $An_{>66}$, but positively correlating at $An_{<66}$ (Fig. 4d). The MgO content of plagioclase will initially correlate with anorthite because the MgO content of melts decreases during fractional crystallization. However, MgO has a relatively fast rate of diffusion ($D = 1 \times 10^{-19}\,m^2\,s^{-1}$ in An_{95} at ~1200°C; LaTourrette & Wasserburg, 1998; Costa & Morgan, 2010) such that magmatic signals have been lost in $An_{>66}$ plagioclase. The correlation observed in crystal rims may represent crystallization shortly prior to eruption such that these crystal rims have had insufficient time to undergo diffusive re-equilibration. The MgO contents of analyses within high-anorthite cores ($An_{>84}$) fall within two distinct populations: one at $0{\cdot}1 \pm 0{\cdot}02$ wt % and one at higher values $0{\cdot}16 \pm 0{\cdot}1$ wt % (marked in Fig. 4d). No other geochemical variables are observed to be correlated with the difference in MgO. The higher MgO compositions occur only in the centre of the largest high-anorthite cores.

Clinopyroxene zonation

Clinopyroxene crystals display normal zoning with Mg# 80–84 in cores and Mg# 64–72 in rims. As with plagioclase, major element zonation is also reflected by trace elements. TiO_2 concentration generally increases from ~0·7 wt % in cores to ~1 wt % in rims (Fig. 4b). An increase in Al_2O_3 from 2 wt % to ~3·4 wt % is also observed. Correlations between Mg# and trace elements are much less strong than between anorthite content in plagioclase and trace elements. Hourglass sector zoning is clearly visible in some clinopyroxene grains and may be accounted for by rapid crystal growth where structural sites do not maintain equilibrium with the melt on different crystal faces (Nakamura, 1973). This leads to greater Mg and Fe uptake on {100} faces than on {010} and {110} faces, which has a concurrent effect of diluting Ca, Al and Ti. Sector zoning accounts for much of the spread in Ti concentration with respect to Mg# observed in Fig. 4b. Compositions of clinopyroxenes that grew in equilibrium with their host melt were selected on the basis of having CaO contents in the range 16–20 wt %, rather than values of <16 wt %, which indicate disequilibrium during growth. Only these compositions were used in subsequent calculations. No evidence for the presence of orthopyroxene exsolution, which could act to reduce CaO content, was observed in BSE images.

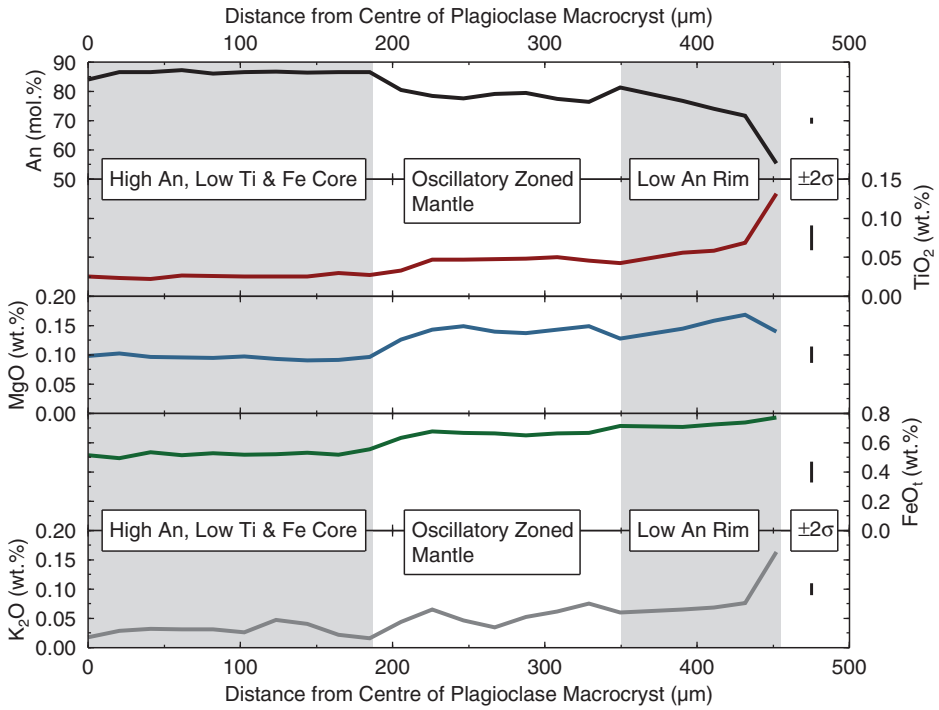

Fig. 6. Typical EMPA profile across a large plagioclase phenocryst from crystal centre (0 μm) to the crystal boundary with the groundmass. The plagioclase is from sample LAK29. Three clear compositional domains are visible: a high-anorthite core, an oscillatory zoned mantle of moderately high anorthite content, and a rim of monotonically decreasing anorthite content. Major element zonation is also reflected by trace elements, particularly TiO_2. Zoning in MgO has been overprinted by diffusion, apart from possibly at the very edge of the crystal rim. Glomerocrystic plagioclase crystals that abut other phenocrysts do not exhibit low-anorthite rims. At the right of the diagram 2σ errors are shown.

Mapping element distributions in plagioclase

Anorthite distribution in plagioclase

Calibrated BSE images of glomerocrysts provide information about the growth of plagioclase crystals in the Laki magma. Figure 7 shows a typical calibrated BSE image of a Laki glomerocryst. High-anorthite cores are found in only the largest grains, which may contain more than one high-anorthite region (i.e. single grains often appear to have multiple nuclei), although the effects of a complex 3D geometry are unconstrained in our 2D analyses. High-anorthite cores show a high degree of homogeneity and have rounded contacts with oscillatory zoned mantles that wrap around them.

Oscillatory zoned mantles display variations in anorthite of 2–5 mol % on scales of 5–25 μm. It is not possible to correlate the same zones across different grains. The amplitude and magnitude of oscillations vary on a grain-to-grain basis, which could be expected during growth in a dynamic magma reservoir (e.g. Ruprecht *et al.*, 2008). Zonation patterns indicate that in many cases single grains became joined during the growth of the oscillatory zoned domain. Joining of grains along boundaries parallel to crystal faces may indicate that aggregation during this phase of crystal growth may have occurred by synneusis rather than crystal settling alone (Schwindinger, 1999).

Crystal mantles are wrapped by low-anorthite rims of variable thickness. Rims form a coating that often encloses numerous distinct mantle ± core 'grains' that often rest at high angles to each other. Rims display normal zoning with a monotonic decrease in anorthite towards the crystal face. In glomerocrysts where plagioclase crystals rest against each other or other phases, rims are reduced or absent and do not reach such low anorthite values as rims adjacent to the groundmass. Glomerocrysts therefore apparently formed prior to the final phase of melt evolution. Groundmass grains have similar anorthite contents to the very edge of macrocryst rims.

Cathodoluminescence (CL) and the distribution of titanium in plagioclase

The intensity of CL images is an indicator of crystal trace element content (Reed, 2005). The high degree of correlation between TiO_2 in plagioclase determined by EMPA and CL intensity ($r^2 = 0{\cdot}95$) suggests that CL images provide a qualitative map of TiO_2 distribution in this phase. Clinopyroxene, olivine and Fe–Ti oxide are not CL active and appear black. Low CL intensities are observed in the core of plagioclase phenocrysts but increase outwards in plagioclase rims and are strongest adjacent to the groundmass and in groundmass grains (Fig. 8). Complex patterns of zoning observed in BSE

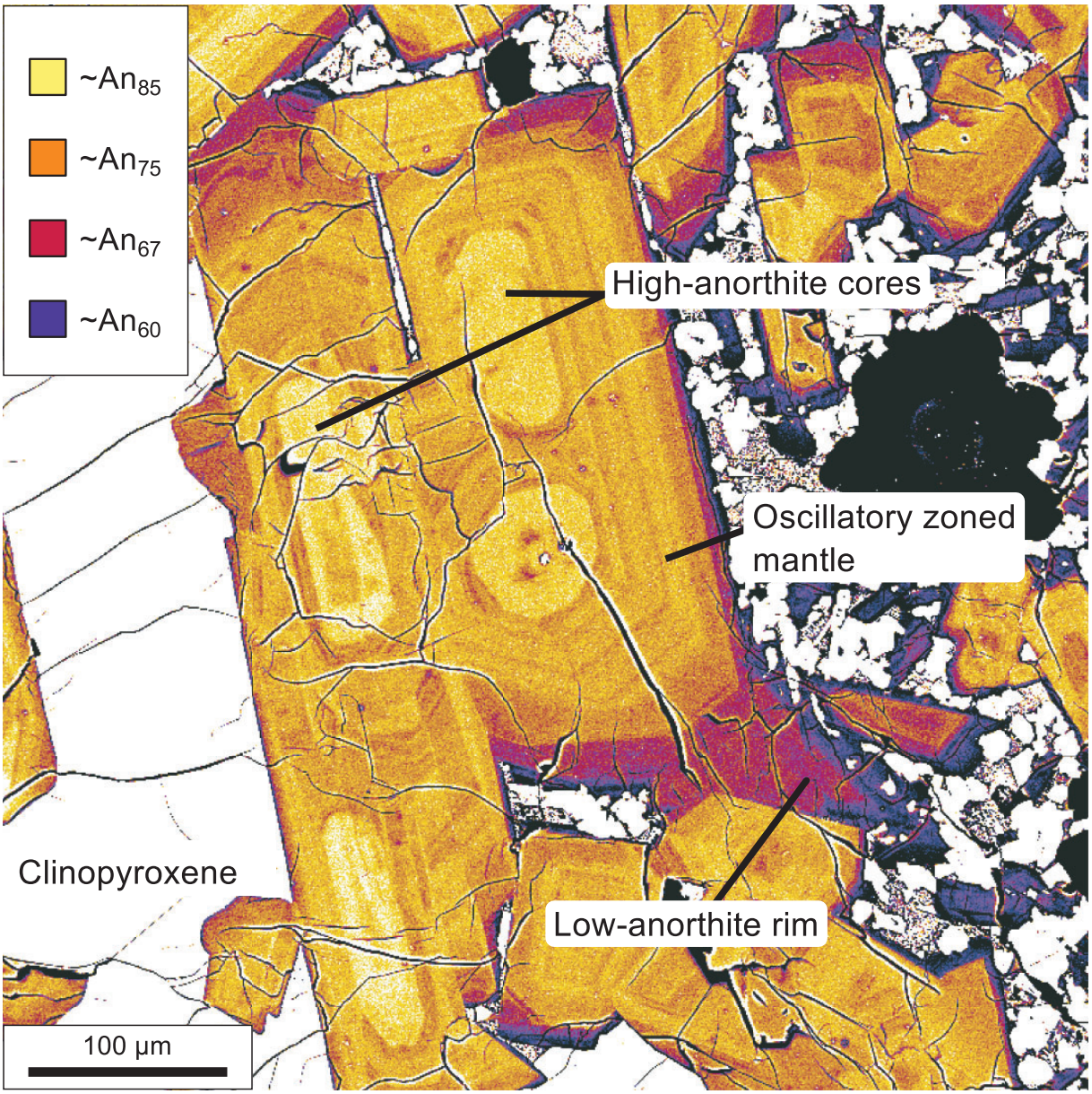

Fig. 7. False colour calibrated backscattered electron image of part of a glomerocryst in sample LAK12. The three plagioclase domains illustrated in Fig. 6 are clearly visible. Most plagioclase–plagioclase boundaries are located within the oscillatory zoned mantle. Oscillatory zoning is particularly clear in the central grain. Zones cannot be traced between grains. Crystal rims wrap around joined grains. It should be noted that low anorthite contents are present only in the rims of crystal boundaries that are in contact with the groundmass; no dark colours are visible between the large central plagioclases, or between them and the large clinopyroxene to the left. Groundmass grains have the same anorthite content as the edges of phenocryst rims.

images are also visible in CL images. High TiO_2 is not observed within grains or at grain boundaries within glomerocrysts.

Crystal size distribution

In addition to compositional information, the crystal size distribution (CSD) of magmas may be used to investigate the conditions experienced during crystallization (e.g. Higgins, 2000). CSDs are particularly sensitive to the degree of magma undercooling (Armienti, 2008) and to magma mixing. Hence magmas with different crystallization histories will have different negative gradients on a plot of crystal size against the natural logarithm of population density (Marsh, 1988; Toothill *et al.*, 2006). Sample LAK04 was selected for CSD analysis because the effects of groundmass crystallization can be mitigated by using a

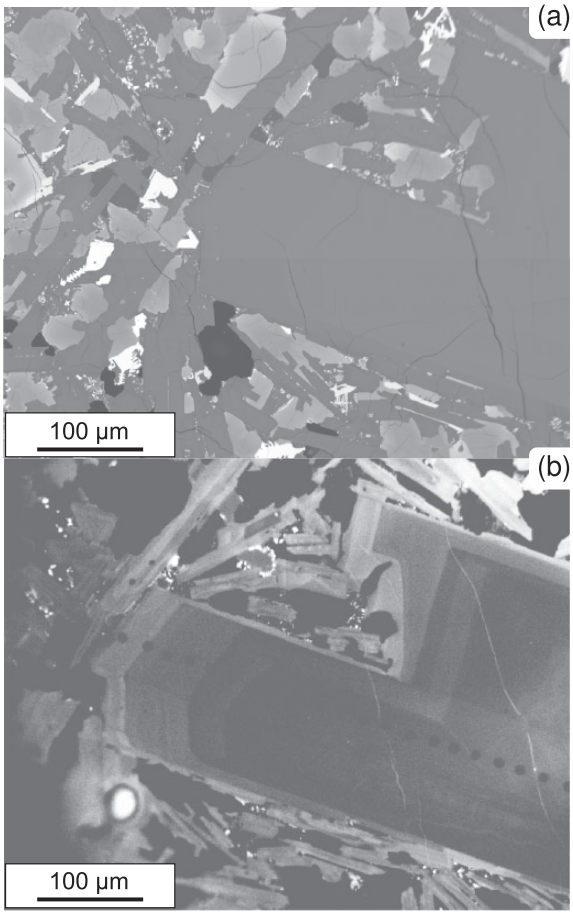

Fig. 8. (a) Unmanipulated BSE image of sample LAK29. Plagioclase is visible as dark grey. Clinopyroxene is mid-grey with lighter grey rims, reflecting Mg# zonation. Olivine is light grey. Small, dendritic groundmass grains of Fe-Ti oxide are visible as the brightest phase. (b) Cathodoluminesence (CL) image of the same sample. High CL activation occurs only in phenocryst rims and groundmass grains that have the highest TiO2 contents. The fine patterns of zonation visible in manipulated BSE images are also visible in CL. The black spots crossing the centre of the grain are points from an EMPA profile.

region where the groundmass is glassy. LAK04 is not texturally anomalous in any other respect.

A continuous plagioclase CSD is observed for crystal sizes <0·05 mm to 1·5 mm (Fig. 9). The distribution is noticeably concave-upwards with a kink at ~0·75 mm. The steepening of the gradient at the smallest crystal sizes (<200 μm) may be the result of degassing-induced crystallization during eruption and lava emplacement (Hammer & Rutherford, 2002). This is consistent with the work of Guilbaud *et al.* (2007), who accounted for abundant groundmass crystallization in Laki lava flows with large undercooling resulting from the loss of ~1 wt % H_2O during eruption. Kinks in CSDs are commonly explained by mixing populations of different crystal size (e.g.

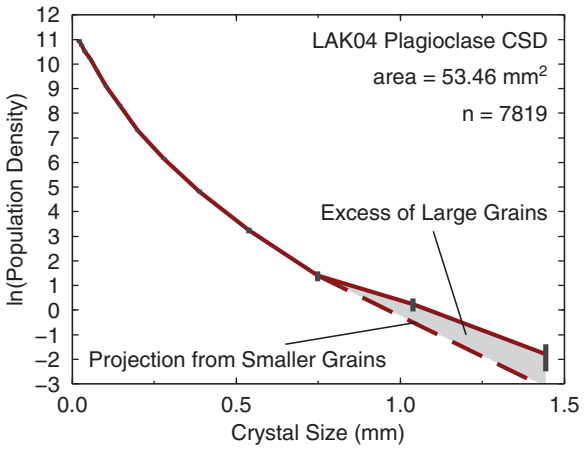

Fig. 9. Crystal size distribution (CSD) of plagioclase grains in the glassy portion of sample LAK04. The gentle concave-up shape of the distribution and the kink at 0·75 mm crystal size should be noted. Projection of the trend at <0·75 mm to larger grain sizes shows that there are more large grains >0·75 mm than would be expected if the CSD were controlled by nucleation and growth alone.

Marsh, 1988). To assess the effect of right-hand truncation effects arising from the scarcity of crystals in large size bins, a CSD using linear size bins was also calculated (see Armienti, 2008). Linear binning reveals that low population densities become problematic only at crystals sizes >1·5 mm and that the break in slope at ~0·75 mm crystal size is a genuine feature of the sample.

DISCUSSION

Concurrent mixing and crystallization recorded in melt inclusions

The similar form of the average melt inclusion REE profile to that of the average of whole-rock profile suggests that the melt inclusions and whole-rock samples are cogenetic (Fig. 5c). The offset of the melt inclusion mean to lower REE concentrations than the whole-rock mean may be explained by trapping of melt inclusions in olivines more forsteritic than those in equilibrium with the carrier liquid and the whole-rock.

Laki olivine-hosted melt inclusions record a statistically robust decrease in La/Yb variability as host forsterite content decreases and hence display the same behaviour as samples from both Borgarhraun and Iceland as a whole (Fig. 5b; Maclennan, 2008*a*). This behaviour has been interpreted as evidence for concurrent mixing and crystallization of diverse mantle melts (variable La/Yb) in magma reservoirs as they cool. The observed diversity in La/Yb cannot be accounted for by differentiation processes and changes in element partitioning. Dissolution–reaction–mixing (DRM) processes have been invoked to explain trace element diversity in $Fo_{>85}$ olivines at various locations including Iceland (e.g. Danyushevsky *et al.*, 2003,

2004). Melt inclusions generated by DRM processes involving plagioclase are predicted to have extremely low La concetrations, low La/Yb and large positive strontium anomalies. Strontium anomalies can be quantified using the Sr/Sr* parameter of Gurenko & Sobolev (2006), where $Sr/Sr^* = Sr_n/(Ce_n/Nd_n)^{0.5}$ and subscript n indicates chondrite normalization values. Sr/Sr* values of Laki melt inclusion are <1 for 120 out of 121 inclusions analysed. Whereas DRM processes are predicted to produce a negative correlation between La/Yb and Sr/Sr*, the Laki observations show a very weak correlation between these ratios ($r = 0{\cdot}098$), indicating that the dominant control on trace element variations in Laki melt inclusions is not DRM. Correlations between trace element and Pb-isotope compositions in Icelandic melt inclusions elsewhere (Maclennan, 2008*a*, 2008*b*) provide further evidence of a mantle control on inclusion trace element compositions.

To compare melt inclusion variability and mixing processes between different eruptions, Maclennan (2008*a*) defined the Þ parameter. Þ is a measure of the deviation of a melt inclusion composition from the average composition of the eruption that it comes from, normalized to the expected standard deviation of original, unmixed end-member melt compositions for the eruption. Laki inclusions lie within the triangular envelope defined by previously studied eruptions on a plot of host olivine forsterite content vs Þ (Fig. 10a; Gurenko & Chaussidon, 1995, 1997, 2002; Slater *et al.*, 2001; Maclennan *et al.*, 2003*a*, 2003*b*; Maclennan, 2008*a*, 2008*b*).

The degree of magma mixing can be defined using the mixing parameter *M*, which ranges from zero for unmixed to unity for complete mixing of passive tracers (Maclennan, 2008*a*). *M* can be calculated as a function of forsterite content using melt inclusion Þ values, which converge towards zero as mixing proceeds. The change of *M* with host olivine forsterite content for all Icelandic melt inclusions, including Laki, is shown in Fig. 10b. These new data allow *M* to be better constrained at lower forsterite contents than previously possible. A sharp increase in *M* is observed as the olivine composition passes through ~Fo_{86}, followed by a slow and steady increase as magma evolves to crystallize Fo_{84} down to Fo_{73}. The modest change in *M* above Fo_{86} is due to mixing during crystallization being balanced by the input of a range of mantle melt compositions. This indicates that the lowest forsterite content of olivine in equilibrium with Iceland mantle melt is about Fo_{86}. Between Fo_{86} and Fo_{83} mixing processes are dominant. The apparent reduced efficiency of mixing at $Fo_{<83}$ may not necessarily reflect slower stirring in reservoirs, but rather indicates that most homogenization of mantle-derived heterogeneity has already taken place. Concurrent mixing and crystallization of parental magmas has therefore occurred in deep regions of the Laki plumbing system in the same manner as elsewhere in Iceland.

Primitive macrocrysts crystallizing from unmixed and diverse parental melts may therefore also preserve a record of growth from melts of variable composition. For example, Winpenny & Maclennan (2011) identified primitive high-Mg# clinopyroxenes in the Borgarhraun flow, which grew from depleted melts before they were stirred into the mixed Borgarhraun carrier liquid. Given that

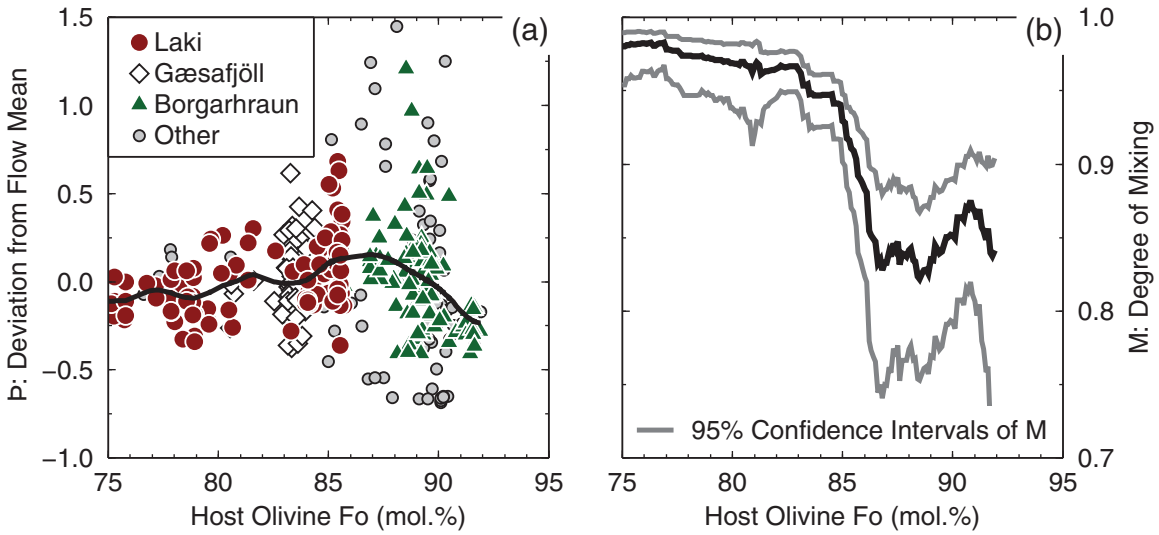

Fig. 10. The record of concurrent mixing and crystallization in the Laki system and in Iceland as a whole. (a) Plot showing the reduction in melt inclusion variability with decreased olivine forsterite content in a series of eruptions and in Iceland as a whole. The parameter Þ is briefly explained in the text and has been fully discussed by Maclennan (2008*a*). The mean inclusion La/Yb at a given host forsterite content is plotted as a black line. (b) Plot showing the variation of the degree of melt mixing [*M*; full description has been given by Maclennan (2008*a*)] with decrease in olivine forsterite content. The grey lines show the 95% confidence interval of the mixing parameter at a given host forsterite content (*M*).

Laki melt inclusions show strong evidence for the presence of variable composition mantle melts, it follows that macrocrysts may also preserve a record of growth from different melt compositions.

High-anorthite plagioclase cores

High-anorthite plagioclase macrocryst cores ($An_{>84}$) are characterized by low TiO_2 and FeO_t, and deviate from trends described by lower anorthite compositions (Fig. 4). Very high anorthite contents have been reported in a recent study of hydrothermally altered Icelandic basalts by Marks *et al.* (2011). In their study hydrothermally derived $An_{90–100}$ plagioclase from the Reykjanes Peninsula was shown to have an MgO content much lower than the range observed at Laki of 0·1–0·16 wt %, which is considered to be magmatic. Furthermore, Laki plagioclase macrocryst cores do not show textural evidence for alteration. A hydrothermal origin for high-anorthite plagioclase in Laki is therefore disregarded. Bindeman *et al.* (2006) and Guilbaud *et al.* (2007) have previously described $An_{>80}$ compositions in the Laki system as xenocrysts. Passmore *et al.* (2012) observed an increase in average plagioclase anorthite content of lavas through the course of the eruption. No changes in zoning are observed between samples of different eruptive phases. The increase in average anorthite content is therefore likely to be driven by an increase in the proportion of macrocrysts bearing high-anorthite cores as the eruption progresses.

Although it has been demonstrated that plagioclase cores are too primitive to be in equilibrium with the carrier liquid, it is unclear whether the cores grew from a melt parental to the carrier liquid or were plucked from the sides of the plumbing system, having crystallized from an unrelated melt in a previous intrusive event. We have used a combination of olivine-hosted melt inclusions, textural information and modelling to address the following questions: Where did the plagioclase cores grow? Are they petrogenetically related to the carrier liquid? In what magmatic environment did plagioclase mantles and rims grow? How are plagioclase composition domains related to olivine and clinopyroxene macrocrysts and to olivine-hosted melt inclusions?

Melt inclusion constraints on the origin of high-anorthite plagioclase cores

Melt Ca/Na and Al/Si are the major controls on plagioclase composition, with high Ca/Na (and Al/Si) stabilizing high anorthite contents (e.g. Elthon & Casey, 1985; Panjasawatwong *et al.*, 1995; Namur *et al.*, 2011). Pressure also exerts a control on anorthite content, with an approximate drop of ~2 mol % anorthite expected per 1 kbar increase in pressure (Danyushevsky, 2001). Conversely, higher H_2O activity increases the equilibrium anorthite content of melt by ~2 mol % per 1 wt % H_2O (Panjasawatwong *et al.*, 1995). Nichols *et al.* (2002) observed that mafic magmas in Iceland contain up to 1 wt % H_2O. In the case of Laki, Guilbaud *et al.* (2007) predicted a pre-eruptive H_2O concentration of ~1 wt % using the plagioclase–melt model of Putirka (2005) as a hygrometer, and Passmore *et al.* (2012) estimated a water content of ~0·75 wt % based on trace element data. The maximum equilibrium anorthite content of Icelandic magmas can be increased only a few mol % by the presence of ~1 wt % H_2O.

To test the feasibility of crystallizing $An_{84–89}$ plagioclase from melts with $Ca/Na < 4$, equilibrium anorthite contents were calculated for a selection of tholeiitic Icelandic melts with $3 < Ca/Na < 4$ using equation (33) of Namur *et al.* (2011). This empirical model is calibrated for anhydrous mafic compositions at 1 atm. The effect of overestimating anorthite content by performing calculations at 1 atm rather than at more realistic storage depths in the mid- to lower crust (e.g. Winpenny & Maclennan, 2011) is likely to outweigh the effect of ignoring H_2O as the melts are relatively dry. This model was primarily selected because of its sole dependence on melt composition and its ability to reproduce the experimental data collated by Namur *et al.* (2011) across the full range of anorthite contents of interest. The models of Panjasawaong *et al.* (1995) and Putirka (2005) were also tested and found to be inappropriate. The Panjasawatong *et al.* (1995) model overestimated the equilibrium anorthite content in $\sim An_{60}$ experimental compositions, but underestimated it in $An_{>80}$ experiments. The Putirka (2005) model reproduced $\sim An_{60}$ experimental compositions well but overestimated compositions at higher anorthite contents of $An_{80–90}$ by up to 10 mol %. Application of the Namur *et al.* (2011) model indicates that $3 < Ca/Na < 4$ melts in Iceland such as the Gæsafjöll and Stapafell glasses of Maclennan (2008*a*) are capable of crystallizing plagioclase in the range $An_{76–80}$. This suggests that the melts from which olivine has grown in the Laki system do not have a sufficiently high Ca/Na to crystallize $An_{84–89}$ at the same time as Fo_{86} olivine.

To confirm that crystallization of $An_{>84}$ from observed Icelandic melt compositions is possible, the Ca/Na of melt inclusions from a range of Icelandic eruptions was plotted together with the Ca/Na of Laki melt inclusions (Fig. 5a). Inclusion data were collated from Gurenko & Chaussidon (1995, 1997, 2002), Slater *et al.* (2001), Maclennan *et al.* (2003*a*, 2003*b*) and Maclennan (2008*a*, 2008*b*). Melt inclusions were filtered for anomalously high Sr/Ce ratios to exclude the small proportion of melts that have been affected by plagioclase digestion. At high host forsterite contents Ca/Na increases to values between four and eight, which suggests that higher anorthite contents may be in equilibrium with these melts.

Some eruptions that have high Ca/Na matrix glass compositions carry high-anorthite plagioclase: Háleyjabunga and Lagafell on the Reykjanes Peninsula (Gurenko &

Chaussidon, 1995) and Kistufell in the Northern Volcanic Zone (NVZ) (Breddam, 2002) have Ca/Na ratios of 4·5–5·5 and 4–4·5 and carry $An_{82–90}$ and $An_{75–89}$ respectively (Figs 5a and 13b). Applying equation (33) of Namur *et al.* (2011) to the matrix glass compositions reproduced $An_{82–89}$. High-anorthite plagioclase in Iceland may therefore crystallize from Icelandic melts with high Ca/Na. The source for these melts, which may be responsible for the generation of high-anorthite plagioclase at Laki, will be discussed below.

Textural constraints on the origin of high-anorthite plagioclase

Further information about the nature of high-anorthite cores may be gleaned from their crystal textures. BSE images of high-anorthite cores show that they are rounded in shape, which suggests that they have undergone some degree of textural evolution and may have been out of equilibrium with their host melt at some point (Fig. 7). Furthermore, high-anorthite cores are never observed to be in contact with the cores of olivine or clinopyroxene macrocrysts. It is possible that resorption may have occurred following entrainment of primitive crystals into a liquid unsaturated in plagioclase, such as a low Ca/Na, enriched mantle melt, prior to the growth of equilibrium oscillatory zoned mantles.

The upward kink in the plagioclase CSD at >0·75 mm crystal length that indicates an excess of large grains (Fig. 9) may be explained by the addition of an accumulated or assimilated population of high-anorthite cores. The cores are found only in larger plagioclase grains and act as nuclei for the growth of oscillatory zoned mantles. Only large grains containing material present in non-equilibrium growth proportions will deviate from the trend expected from crystal nucleation and growth. Textures and CSD analyses hence suggest that the high-anorthite cores are not simply related to the carrier liquid and appear to have been added to Laki magma at an early stage of its evolution so that no record of the melts from which they crystallized remains.

Constraints on the origin of plagioclase mantles

Plagioclase macrocryst mantles are in equilibrium with the range of compositions observed in olivine-hosted melt inclusions. It is therefore probable that they grew from melts parental to the carrier liquid. However, the mantles do not show simple normal zoning with steadily decreasing anorthite content, as would be expected if they grew in a system evolving purely by fractional crystallization along a single liquid line of descent. Instead, they show prominent oscillatory zoning (Fig. 7). Such oscillatory zoning has previously been interpreted as being the result of mixing of melts that have experienced varying degrees of fractional crystallization (e.g. Ginibre *et al.*, 2002*a*). This interpretation implies that a consistent primitive melt composition has been added and that mixing occurs with melts that have all followed the same fractional crystallization path. However, it has been demonstrated that the trace element content of olivine-hosted melt inclusions in equilibrium with plagioclase mantles is highly variable. La/Yb variability has been interpreted as the result of mantle melt diversity. It has been demonstrated that Icelandic melts of different trace element content have different major element compositions, including CaO and Na_2O (Shorttle & Maclennan, 2011). It is therefore plausible that oscillatory zoning may result from crystallization of plagioclase from melts in equilibrium with $Fo_{84–86}$ but with otherwise variable compositions.

As previously discussed, the anorthite content of plagioclase is controlled not only by melt composition (Panjasawatwong *et al.*, 1995; Namur *et al.*, 2011) but also by melt H_2O content (e.g. Sisson, 1993; Putirka, 2005). The direct role of melt CO_2 content upon plagioclase composition is not well understood, but nevertheless it is likely that changes in the volatile contents of the melts caused by degassing or gas flushing can drive shifts in plagioclase anorthite content that are independent of the major element composition of the melt. Oscillatory zoning in plagioclase may thus be driven by variations either in major element composition or in H_2O–CO_2 content of the melt. Therefore to confirm that either mixing of variably fractionated melts or mingling of diverse mantle melts is causing oscillatory zoning, the effect of H_2O–CO_2 needs to be ruled out. Oscillations of ~1 mol % amplitude and ~1 μm wavelength result from kinetic effects on grain boundaries during crystal growth (Ginibre *et al.*, 2002*b*). Zones on this scale are too small to be resolved using the techniques employed here and are not considered further.

To test the role of H_2O-CO_2 content in controlling zoning, EMPA crystal profile data that were collected at known spacings of ~10 μm were collated from regions of oscillatory zoning identified in BSE images. For each profile the differences in anorthite and TiO_2 (ΔAn & ΔTi) were calculated for each possible unique pairing of probe points. For example, for a profile consisting of points numbered 1, 2, 3 and 4, differences would be calculated between 1 & 2, 1 & 3, 1 & 4, 2 & 3, 2 & 4 and 3 & 4.

ΔAn & ΔTi from all profiles are presented on a plot of point spacing in μm vs ΔTi/ΔAn (Fig. 11). The degree and nature of correlation between anorthite and TiO_2 may therefore be determined at different length scales in zoned crystals. If anorthite and TiO_2 correlate positively, then ΔTi/ΔAn will be positive; if they correlate negatively, then ΔTi/ΔAn will be negative. A decrease in TiO_2 coupled with an increase in anorthite indicates that zones of higher anorthite content grew in melts with higher Ca/Na and lower TiO_2, and zones of lower anorthite content in melts with lower Ca/Na and higher TiO_2. If

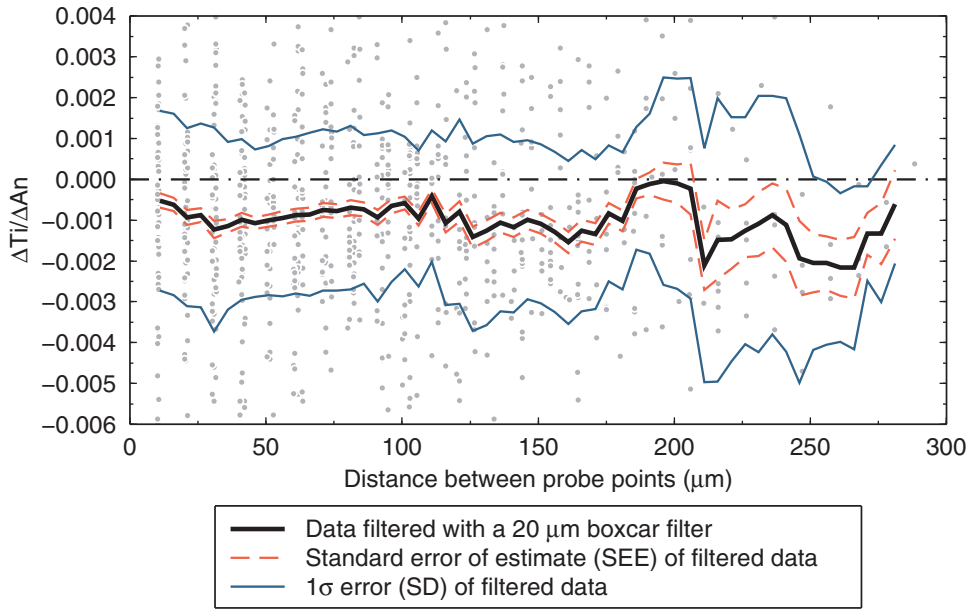

Fig. 11. Plot showing how correlation of TiO_2 and anorthite varies as function of distance between EMPA points in oscillatory zoned mantles of plagioclase grains. Positive ΔTi/ΔAn values indicate a positive correlation and negative values a negative correlation. The mean ΔTi/ΔAn at all lengthscales is reliably negative, which suggests that anorthite and TiO_2 variation are coupled.

variations in anorthite were the result of changes in H_2O content alone then TiO_2 in the melt and plagioclase would continue to increase independently of plagioclase composition, which would oscillate, resulting in a breakdown of the negative correlation of anorthite with TiO_2, especially at short length scales (Fig. 12).

The ΔTi/ΔAn data presented in Fig. 11 show a large spread of values. Filtering with a 20 μm boxcar filter shows that the data cluster strongly at ΔTi/ΔAn = −0·001 at all lengthscales. Calculation of the standard error of estimate (SEE) of the filtered data indicates that despite this spread, negative correlation of anorthite with TiO_2 consistently occurs in oscillatory zoned regions. This correlation suggests that oscillatory zoning in plagioclase mantles is caused by variations in melt major element composition (i.e. Ca/Na). This is further supported by the presence of zoning in K_2O, which is visible in Fig. 6: Putirka (2005) demonstrated that the orthoclase component of plagioclase is independent of H_2O content and depends on melt composition alone.

Melt composition may change as the result of mixing of variably fractionated melts or by supply of variable mantle melts into the system from depth. By plotting melt inclusion La/Yb against Ca/Na and shading by host forsterite content it is possible to distinguish between these two options (Fig. 5d). As melt inclusion Ca/Na drops, a concurrent drop in host forsterite content is observed. However, there is no variation of Ca/Na with La/Yb in olivines of constant forsterite content, as would be expected if Ca/Na was varying as a result of supply of variable melts. This indicates that the degree of melt fractionation is the main control on melt Ca/Na and consequently the development of oscillatory zoning in the plagioclase. Indeed, the convergence in La/Yb with decreasing Ca/Na mirrors that which occurs with decreasing host forsterite content. It is therefore likely that the Laki magma experienced numerous recharge events by melts in equilibrium with $Fo_{\leq 86}$ with variable La/Yb but similar Ca/Na that underwent subsequent crystallization and mixing. However, it is not possible to rule out the possibility that crystals grew whilst being transported around a compositionally zoned magma reservoir.

Modelling the evolution of the Laki magma

Accurate prediction of equilibrium plagioclase anorthite, clinopyroxene Mg# and olivine forsterite contents from a melt composition requires the SiO_2, Al_2O_3, CaO, Na_2O, FeO and MgO content of the melt to be well constrained. Using melt inclusion major element compositions that have experienced post-entrapment crystallization or overheating during re-homogenization is therefore not a reliable method for predicting the equilibrium crystal contents of parental Laki melts. To test the ability of a single liquid line of descent to reproduce the full suite of Laki macrocryst compositions, a forward modelling approach was undertaken to predict the evolution of melt composition during fractional crystallization.

Petrolog3 modelling

Initial fractional crystallization calculations were performed using the program Petrolog3 (Danyushevsky & Plechov, 2011). The program makes use of a range of

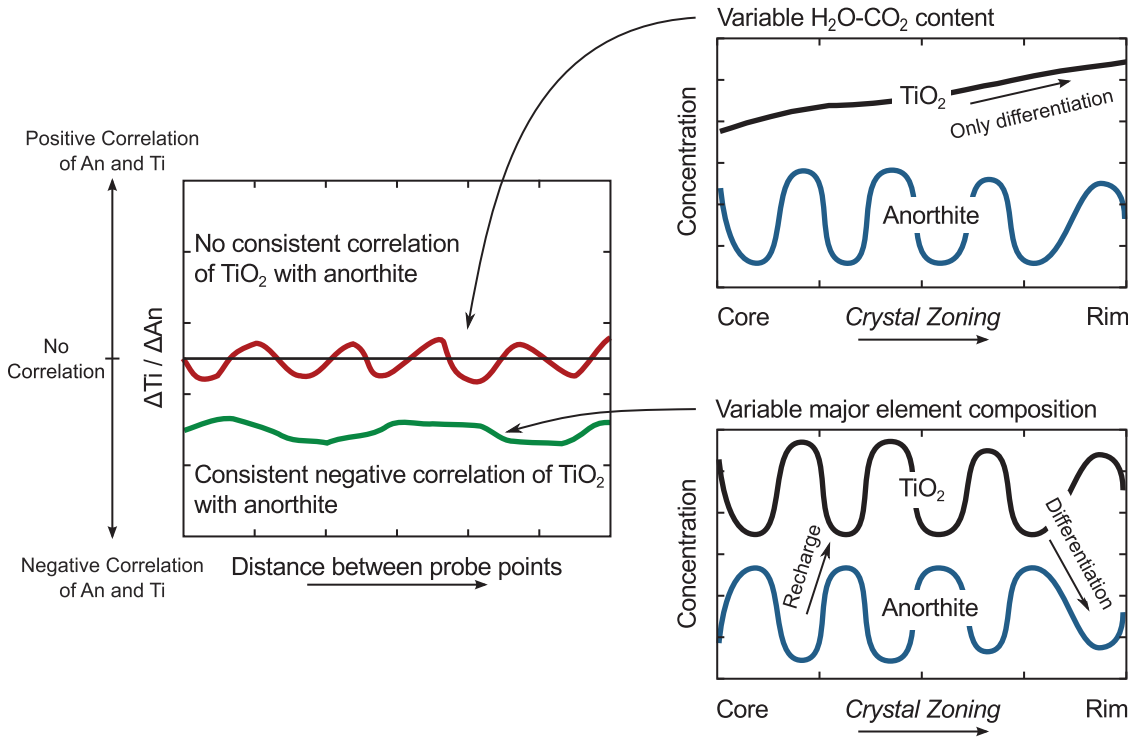

Fig. 12. Schematic illustration of the principles behind the method used to investigate the environment of plagioclase mantle growth. Top right: if oscillations in anorthite content were driven by variations in the H_2O–CO_2 content of magmas, in turn driven by CO_2 degassing or flushing, then there will no correlation between anorthite content and TiO_2, which is a tracer of the degree of melt evolution. Bottom right: if oscillations were driven by variations in melt composition then TiO_2 will correlate negatively with anorthite content because primitive melts crystallize higher-anorthite plagioclase, but contain lower TiO_2 than more evolved melts. Left: the degree of correlation can be expressed in terms of $\Delta Ti/\Delta An$, which will hover around zero for no correlation, and will be less than zero for negative correlations.

published mineral–melt equilibrium models to calculate the composition and proportion of melt and crystals during crystallization or reverse crystallization at specified conditions. The starting melt composition used for all Petrolog3 calculations was an average of the tephra glass composition of Passmore *et al.* (2012) and is given in Table 1. Reverse fractional crystallization calculations were performed at 0·001, 2, 4 and 6 kbar to cover the likely range of pressures at which the evolution of the Laki magma may have occurred. Model runs were performed at an fO_2 of one log unit below the QFM buffer using the full range of plagioclase models available, the Danyushevsky (2001) model for clinopyroxene and the Danyushevsky (2001) model for olivine, with $K\mathrm{d}^{\mathrm{ol-liq}}_{\mathrm{Mg-Fe}}$ fixed at 0·3. To reproduce the observed compositional ranges of the macrocrysts the following phase compositions were not permitted: plagioclase of $An_{>90}$, clinopyroxene of Mg# >84 and olivine of $Fo_{>86}$. Results using the model of Danyushevsky (2001) for plagioclase are presented in Fig. 13a, b and f. Melt TiO_2 composition ranges predicted from crystal compositions using appropriate partition coefficient ranges for basalts at ~1200°C are also shown in Fig. 13a and e. A partition coefficient of $0{\cdot}04 \pm 0{\cdot}01$ was used for plagioclase (Bindeman & Davis, 2000) and $0{\cdot}45 \pm 0{\cdot}1$ for clinopyroxene (Wood & Blundy, 1997; Hill *et al.*, 2010). These ranges bracket the likely maximum errors in partition coefficients.

Low-pressure runs are best at reproducing the composition of macrocryst rims (~An_{60}, cpx Mg# ~72, ~Fo_{70}). The 2 kbar run best matches the crystal composition data, which are consistent with the 1–2 kbar estimation for last melt–crystal equilibration from application of the Yang *et al.* (1996) barometer (see subsequent thermobarometry section). In all models clinopyroxene joins the liquidus when the melt reaches a composition in equilibrium with ~Fo_{83}. Crystallization from Fo_{86} to Fo_{83} is along the ol–plg cotectic. In all cases, including 0·001 kbar, $An_{>84}$ cannot be generated in the presence of $Fo_{<86}$. No plagioclase models in Petrolog3 predict anorthite contents any more than ~1 mol % higher than the Danyushevsky (2001) model. Modelling results therefore suggest that high-anorthite plagioclase cores cannot be generated from a parental melt related to the carrier liquid by a single liquid line of descent. Plagioclase macrocryst mantles and rims, olivine macrocrysts and clinopyroxene macrocrysts may, however, be related to the carrier liquid.

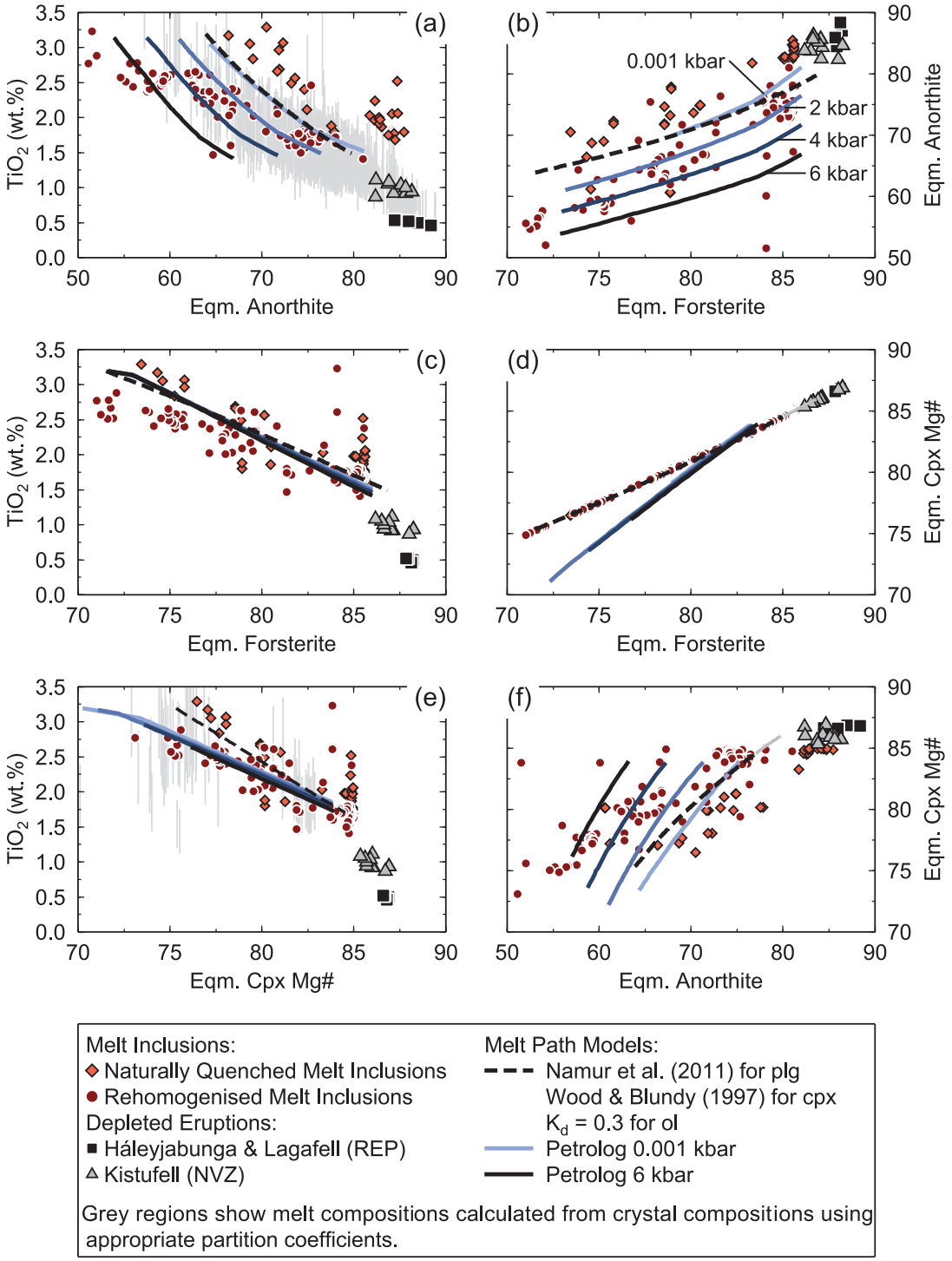

Fig. 13. Plots summarizing the results of modelling the evolution of the Laki magma. Melt evolution paths calculated with PETROLOG3 are presented with the results of our own reverse fractional crystallization model. Labels in panel (b) indicate the pressure of different PETROLOG3 runs; full details of our model set-up are given in the text. Our model using the 1 atm model of Namur *et al.* (2011) shows good agreement with the 0·001 kbar run of PETROLOG3, apart from clinopyroxene Mg#. Calculated equilibrium mineral compositions of eruptions containing (near) equilibrium high-anorthite plagioclase from Háleyjabunga and Lagafell (Gurenko & Chaussidon, 1995) and Kistufell (Breddam, 2002) are plotted for comparison. Equilibrium mineral compositions are also plotted for both naturally quenched and re-homogenized melt inclusions. It should be noted that the naturally quenched inclusions broadly have a similar slope to calculated model paths but are offset to higher anorthite and TiO_2 as the result of post-entrapment crystallization. The effects of re-homogenization are more complex and re-homogenized melt inclusions do not lie along melt evolution paths, but cut across them.

PETROLOG3 uses partition coefficients to constrain the behaviour of elements that are not used in mineral–melt calculations (Danyushevsky & Plechov, 2011). This technique is limited by the quality of partition coefficient models. In the case of Laki a large number of crystal analyses have been collected across the range of mineral compositions. A reverse crystallization model that uses measured crystal compositions to alleviate errors from predicting crystal compositions was constructed to test the reliability of the PETROLOG3 results.

Reverse crystallization model

The average tephra glass composition of Passmore *et al.* (2012) (Table 1) was used as a starting composition for calculations. Melt compositions were held at an fO_2 of one log unit below the QFM buffer throughout. Equilibrium plagioclase anorthite was determined using the model of Namur *et al.* (2011). This model provides a maximum anorthite content because it is calibrated at 1 atm. Equilibrium clinopyroxene Mg# was determined using the model of Wood & Blundy (1997) and equilibrium olivine forsterite was determined using a Kd_{Mg-Fe}^{ol-liq} of 0·3 (Roeder & Emslie, 1970). The temperature-independent model of Wood & Blundy (1997) was chosen in preference to equation (35) of Putirka (2008), which was employed during thermobarometric calculations (see below) to avoid imposing extra conditions on the calculation. A database of all Laki crystal analyses with good totals and stoichiometry was filtered for compositions within ±1 mol % of the calculated equilibrium values for the melt. The proportions in which phases were added back were calculated using the parameterization of the Olivine–Plagioclase–Augite–Melt (OPAM) boundary location from Yang *et al.* (1996) in the case of eutectic (ol + plg + cpx) reverse crystallization. An assemblage of 70% plg + 30% ol was used in the case of cotectic (ol + plg) reverse crystallization (Grove *et al.*, 1992). Average compositions of phases for which measured crystal compositions could be successfully matched were then added in appropriate proportions to the starting melt in increments of 0·1%. The melt composition was then renormalized to 100% and the equilibrium crystal matching process was repeated. Iterations continued while either ol + plg + cpx or ol + plg could be successfully matched. As soon as either plagioclase or olivine could not be matched by measured compositions the model was stopped.

Results of the model are plotted alongside the PETROLOG3 modelling results in Fig. 13. Model results generally reproduce macrocryst rim compositions well and show a good agreement with the 0·001 kbar run of PETROLOG3 for plagioclase at all but the most primitive compositions, where PETROLOG3 predicts anorthite contents a few mol % higher. Olivine forsterite content also shows good agreement, but clinopyroxene Mg# shows divergence. The divergence is retained when a fixed $Kd_{Mg-Fe}^{cpx-liq}$ of 0·26 is used (Toplis & Carroll, 1995) and may be attributed to the clinopyroxene model of Danyushevsky (2001) using an effective $Kd_{Mg-Fe}^{cpx-liq}$ of ~0·3, which is much higher than that calculated using the model of Wood & Blundy (1997) or proposed by Toplis & Carroll (1995). Furthermore, the major element content of clinopyroxene at a given Mg# calculated using the Danyushevsky (2001) model shows significant compositional differences in CaO and Al_2O_3 content of the order of 2–3 wt % with respect to the measured crystals. This deviation indicates that the Danyushevsky (2001) model is poor at determining clinopyroxene compositions in systems of Laki-like composition. To test the sensitivity of the model to varying phase proportions, a number of runs with reasonable fixed phase proportions were performed by varying the phase proportions determined from the point counting data of Passmore *et al.* (2012) (plg:ol:cpx of 57:11:32) by ±5%. Variations of this magnitude did not greatly affect the model results such that the predicted plagioclase anorthite content reached a maximum of ~An_{82} only at an equilibrium olivine composition of Fo_{86}.

Further modelling

Runs were also performed using PETROLOG3 and our own reverse crystallization model without imposing a maximum forsterite content of Fo_{86} to investigate possible equilibrium relationships between high-anorthite plagioclase and olivine. Above Fo_{86} olivine compositions were predicted using stoichiometry based on a Kd_{Mg-Fe}^{ol-liq} of 0·3 (Roeder & Emslie, 1970). Our model suggests that ~An_{86} would be in equilibrium with ~Fo_{90}. PETROLOG3 is capable of producing $An_{>80}$ in equilibrium with ~Fo_{90} only at pressures of less than 4 kbar. The plagioclase, olivine and melt compositions of the depleted eruptions of Háleyjabunga and Lagafell (Gurenko & Chaussidon, 1995) and Kistufell (Breddam, 2002), were broadly reproduced with these low-pressure reverse crystallization models. It is likely that high-anorthite plagioclase grew during cotectic crystallization with high-forsterite olivine. Possible explanations for the absence of high-forsterite olivine from the Laki magma will be discussed below.

Summary of modelling

In summary, modelling using both PETROLOG3 and our own reverse crystallization model suggests that macrocryst rim compositions are close to equilibrium with the carrier liquid composition at low pressures. Most of the range of macrocryst compositions can be described by adding ol + plg + cpx then ol + plg back into the carrier liquid. In low-pressure models the most forsteritic olivine is in equilibrium with the most anorthitic composition of plagioclase mantles. However, high-anorthite macrocryst core compositions are not reproduced. A combination of textural information, CSD analysis, melt inclusion data and modelling of magma evolution paths indicates that

high-anorthite cores are not simply related to the carrier liquid by a single liquid line of descent. They are likely to have crystallized from high Ca/Na melts, which are not observed in olivine-hosted melt inclusions. Therefore it is important to assess where they may arise and how they may relate to the carrier liquid.

Diverse mantle melts and low-pressure crystallization paths

Trace element variability in olivine-hosted melt inclusions and the presence of high-anorthite cores in plagioclase macrocrysts provide evidence for a diversity of primitive melts in the Laki system. The excess of large plagioclase crystals shown by CSD analysis may be explained by accumulation of plagioclase in a melt subsequently mixed into a parental melt or by addition of plagioclase crystallizing on walls deep in the Laki plumbing system. Assimilation of high-anorthite plagioclase as xenocrysts has previously been suggested by Halldorsson *et al.* (2008) as an explanation for Sr-isotope disequilibrium between plagioclase macrocryst cores and groundmass in the Thjórsárhraun lava flow, also in the EVZ of Iceland. Those workers demonstrated that $An_{>80}$ plagioclase crystals with $^{87}Sr/^{86}Sr$ mainly in the range 0·70305–0·70310 could not be cogenetic with the groundmass they were hosted in, which has $^{87}Sr/^{86}Sr$ mainly in the range 0·70315–0·70320.

High-anorthite plagioclase crystals that are close to being in equilibrium with their carrier melts have been reported elsewhere in Iceland, such as Borgarhraun (Winpenny & Maclennan, 2011), Háleyjabunga and Lagafell (Gurenko & Chaussidon, 1995), and Kistufell (Breddam, 2002). These systems are all of depleted composition, with low LREE/HREE ratios. This observation is also consistent with high-anorthite plagioclase being associated with a more depleted Sr-isotope signature than the groundmass in the Thjórsárhraun lava. A recent study of the major element composition of melts associated with depleted and enriched primitive melts in Iceland indicates that whereas depleted melts are associated with high Ca/Na, enriched melts are associated with low Ca/Na (Shorttle & Maclennan, 2011). Indeed, the association of high Ca/Na with depleted melt compositions and high-anorthite plagioclase has been well known in mid-ocean ridge basalt (MORB) for some time (Bender *et al.*, 1978; Elthon & Casey, 1985, and references therein). Plagioclase macrocryst cores, however, solely have high-anorthite contents: no comparable homogeneous, resorbed macrocryst cores are observed with low anorthite contents corresponding to an enriched mantle end-member with low Ca/Na. Given the evidence for the supply of variable mantle melts in the Laki system from olivine-hosted melt inclusions, it is unexpected that a corresponding range of macrocryst cores is not present.

A conceptual framework for understanding the presence of cores solely of high-anorthite composition concerns the way in which polybaric melting proceeds to generate depleted and enriched mantle melts. Enriched mantle lithologies are more fusible than depleted lithologies and will therefore start melting at the base of the upwelling melting column (e.g. Shorttle & Maclennan, 2011). Refractory, depleted lithologies, on the other hand, will not start to melt until the mantle reaches shallow depths. Takahashi & Kushiro (1983) demonstrated that the ol–cpx–opx–melt eutectics of mantle peridotite move away from the olivine apex and towards the plagioclase apex of an ol–plg–qz phase diagram as the pressure of melting decreases. This is consistent with the greater CaO content of shallow depleted melts illustrated by Shorttle & Maclennan (2011). Low-pressure eutectic mantle melt compositions hence lie much closer to the ol–plg cotectics at crustal pressures than high-pressure eutectic melt compositions. Depleted melts are thus closer to plagioclase saturation than enriched melts, resulting in early crystallization of high-anorthite plagioclase. Lower anorthite plagioclase cores are thus absent from macrocrysts, because enriched melts do not saturate in plagioclase until late in their evolution. A similar explanation for the occurrence of high-Mg# clinopyroxene associated with depleted melt compositions in the Borgarhraun flow was proposed by Winpenny & Maclennan (2011): depleted melts saturate much sooner in clinopyroxene and thus crystallize clinopyroxene with Mg# 90 with olivine, while enriched melts are crystallizing only olivine. Further study into the crystallization paths of different mantle melts and their associated plagioclase compositions is currently under way.

A further complication relating to the presence of high-anorthite plagioclase concerns the absence of correspondingly high-forsterite olivine in the Laki system. By contrast, olivines from Háleyjabunga on the Reykjanes Peninsula, which erupted plagioclase macrocrysts up to An_{90}, have olivine macrocrysts with compositions up to $Fo_{91·5}$ (Gurenko & Chaussidon, 1995). Three possible explanations for this contrast, which need not be mutually exclusive, are as follows.

(1) Olivines of up to Fo_{90} have been reported in Laki by Bindeman *et al.* (2006), suggesting that rare primitive olivines may indeed be present. However, no compositions in excess of Fo_{86} were measured in the 54 samples analysed in the present study and by Passmore *et al.* (2012), indicating that if such olivines are present they are exceptionally rare, especially in comparison with high-anorthite cores.

(2) The rate of NaSi–CaAl interdiffusion in plagioclase is much slower than the rate of Mg–Fe interdiffusion in olivine: diffusion coefficients at 1150°C for NaSi–CaAl interdiffusion in plagioclase lie in the range 1×10^{-21} to $1 \times 10^{-25}\,m^2\,s^{-1}$, whereas diffusion coefficients for Mg–Fe interdiffusion in olivine lie around $1 \times 10^{-17}\,m^2\,s^{-1}$. Simple calculations using equation

(9) from Zhang (2010) indicate that >250 kyr are required for significant NaSi–CaAl interdiffusion to take place on a 100 μm lengthscale, whereas only ~10 years are required for significant Mg–Fe interdiffusion. It is therefore likely that high-forsterite olivines have undergone complete diffusive re-equilibration, whereas high-anorthite plagioclases have retained zones of highly primitive composition. However, significant amounts of diffusive re-equilibration of MgO and FeO since the crystallization of Fo_{86} olivine appears unlikely because the correlations between trace element variability and forsterite content shown in Figs 5b and 10 would break down if olivine compositions had been reset.

(3) During transport of depleted melts from deep reservoirs to the sites of melt mixing, a density filter may have acted to separate forsteritic olivine from melt and anorthitic plagioclase. Simple melt density calculations using the molar volumes of Lange & Carmichael (1990) and Lange (1997) indicate that the Háleyjabunga glass of Gurenko & Chaussidon (1995), which is in equilibrium with high anorthite and forsterite contents, has a density of 2·699 Mg m^{-3}. Using the data of Smyth & McKormick (1995) Fo_{88} has a density of 3·573 Mg m^{-3} whereas An_{88} has a density of 2·746 Mg m^{-3}. Olivine is therefore likely to sink out of the melt and be deposited in cumulate bodies, from which it is not remobilized. Plagioclase, however, remains close to neutral buoyancy and may be carried with the melt to shallower levels.

The composition of all the magmatic components of the Laki magma cannot be explained by evolution along a single liquid line of descent from a single primary melt. Depleted and enriched mantle melts, which are likely to have initially different crystallization histories because of their different compositions, have been supplied to the base of the plumbing system but have become mixed together to eventually generate the erupted carrier liquid. To constrain the depths at which these magmatic processes took place both melt barometry and clinopyroxene thermobarometry were employed.

Melt barometry

The location of the olivine–plagioclase–augite–melt (OPAM) boundary in composition space varies as a function of pressure in basaltic magmas (Yoder & Tilley, 1962; Grove, 1993; Yang *et al.*, 1996). It is therefore possible to determine the pressure at which the melt was last in equilibrium with olivine, plagioclase and augite. Point counting results from the recent study of Passmore *et al.* (2012) confirm that Laki samples contain olivine, plagioclase and augite in near-eutectic proportions (with a slight excess in primitive plagioclase suggested by CSD analysis) and that equilibrium between the OPAM phases will have occurred.

Mineral norms calculated from tephra glass compositions using the scheme of Grove (1993) were compared with normative mineralogies recalculated from the same starting composition at a range of pressures using the parameterization of Yang *et al.* (1996) to determine the last pressure of mineral–melt equilibration.

Tephra glass compositions record equilibrium pressures mainly within a range of 1–2 kbar (Fig. 14) with a likely error of the order of 1 kbar. This result indicates that the melt was last in equilibrium with olivine, plagioclase and clinopyroxene within the depth range of 0–9 km in the shallow crust. However, only the outermost crystal rims record compositions in equilibrium with tephra glass compositions according to the modelling results. To investigate the physical conditions experienced earlier in the crystallization history, a different approach was employed making use of more primitive clinopyroxene core compositions.

Clinopyroxene thermobarometry

Clinopyroxene thermobarometers were used to determine the pressure and temperature conditions experienced in the course of clinopyroxene crystallization from the Laki magma. However, because most clinopyroxenes occur in glomerocrysts associated with both plagioclase and olivine it is reasonable to infer that these phases experienced the same conditions of crystallization. A number of clinopyroxene-based thermobarometers are now available and have been reviewed by Putirka (2008). The thermobarometers with the smallest errors make use of carefully selected equilibrium clinopyroxene–melt pairs (Putirka, 2008). At Laki, both tephra glass and whole-rock compositions are far from equilibrium with most observed clinopyroxene compositions (Fig. 3). Equilibrium melts have therefore been determined by matching compositions from a large database ($n = 2495$) [see appendix 1 of Shorttle & Maclennan (2011) for a list of data sources] of Icelandic magmas (glass and whole-rock analyses) to clinopyroxene compositions in a manner similar to that employed by Winpenny & Maclennan (2011). The database of Icelandic magmas was edited to contain only samples from rift zones. Flank zone compositions were discarded because they erupt alkali and transitional basalts, which are inappropriate to compare with the tholeiitic Laki system (Sigmarsson & Steinthorsson, 2007). Any whole-rock samples that contain more than 12 wt % MgO were also removed as these are likely to have undergone olivine accumulation.

Initially each clinopyroxene analysis was tested for Mg–Fe and Ti equilibrium with all melts. $K\mathrm{d}_{\mathrm{Mg-Fe}}^{\mathrm{cpx-liq}}$ was calculated using the temperature-dependent equation (35) of Putirka (2008). D_{Ti} was calculated using the composition-, temperature- and pressure-dependent

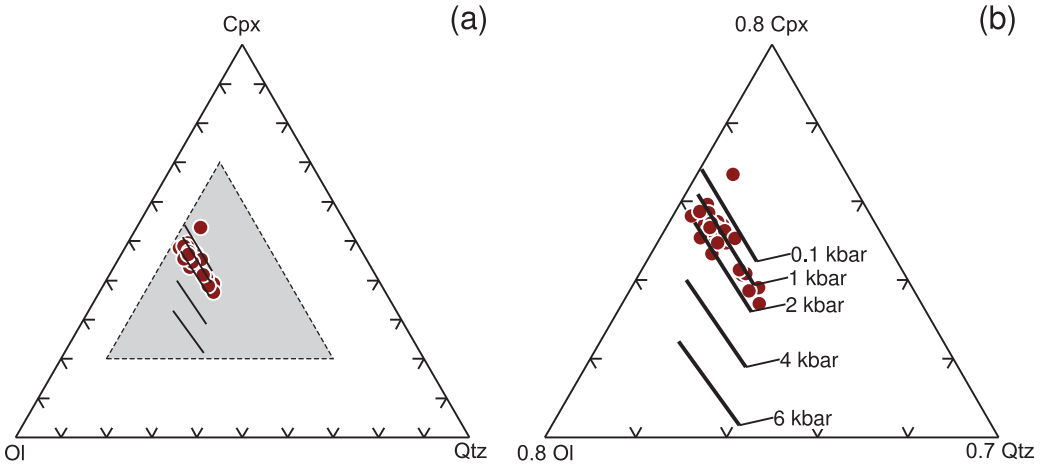

Fig. 14. Normative mineralogy of Laki tephra glass calculated using the method of Grove (1993) and OPAM boundary locations (lines) calculated using the method of Yang *et al.* (1996) projected onto the olivine(Ol)–diopside(Cpx)–quartz(Qtz) plane from plagioclase. The left-hand end of each OPAM-boundary line represents the most primitive sample and the right-hand end the most evolved. Tephra glass compositions, which represent the carrier liquid, were last in equilibrium with plagioclase, clinopyroxene and olivine at ~1–2 kbar ± 1 kbar in the shallow crust. (b) Enlarged view of the shaded area in (a).

parameterization of Hill *et al.* (2010). Thresholds of ±10% were used for both Mg–Fe and Ti equilibrium, which are larger than model errors. Suitable initial pressure and temperature estimates were determined by repeat calculations. Pressure and temperature estimates for each clinopyroxene–melt pair were then determined by iteratively solving equations (32c) and (32d) of Putirka (2008). The parameterizations of Putirka (1999) were then used to calculate the predicted clinopyroxene CaTs component from the melt composition in each matched clinopyroxene–melt pair. Predicted CaTs was compared with observed CaTs and pairs that were greater than 10% away from CaTs equilibrium were discarded. Filtering by CaTs was used because the Putirka (2008) barometer is sensitive to the Al_2O_3 content of pyroxene. Pressure and temperature were then re-calculated using only the clinopyroxene analyses that met Mg–Fe, Ti and CaTs equilibrium criteria and the initial pressure and temperature estimates as starting conditions.

A total of 15 clinopyroxene analyses were successfully matched to between 20 and 200 melts, which are supplied in Supplementary Data Electronic Appendix 4. Matched melts were drawn from a range of eruptions containing 7–9 wt % MgO such as Gæsafjöll in the Theistareykir system, Thjórsárhraun in the Bárðarbunga system and Bláfjall in the Fremrinámur system. The standard deviation of the pressures and temperatures calculated for each clinopyroxene analysis is much less than the ±1·5 kbar and ±30 K errors of the models (Putirka, 2008). Most clinopyroxenes record pressures in the range 3·5–6·9 kbar, with one recording 2·2–3·4 kbar (Fig. 15). These pressures correspond to a maximum temperature range of 1171–1190°C in the high-pressure samples and 1150–1160°C in the low-pressure sample. The low pressure is recorded in the lowest Mg# analysis from a crystal rim and lies close to the pressure range predicted using OPAM boundary barometry. This method of melt matching and pressure calculation was tested using clinopyroxene data for Borgarhraun, North Iceland. The 6–10 kbar pressure range reported by Winpenny & Maclennan (2011), who used a different clinopyroxene–melt matching technique combined with the Putirka *et al.* (1996) thermobarometer, is reproduced using the method presented here.

The various models presented by Putirka (2008) were largely calibrated for anhydrous systems using data from 1 atm and 8–40 kbar. The validity of using these thermobarometers in the 2–6 kbar range was tested with data from experiments performed in the 1–8 kbar range that produced coexisting basaltic melt and clinopyroxene. Data were compiled from Tormey *et al.* (1987), Grove *et al.* (1992), Feig *et al.* (2006, 2010) and Villiger *et al.* (2007). However, data in this pressure range are scarce because of technical limitations (e.g. Villiger *et al.*, 2007). For samples in the range 2–5 kbar, the average residual between observed and calculated pressures is 1·5 kbar using the 18 relevant experiments. This suggests that the thermobarometer of Putirka (2008) may overestimate pressures in the range of interest by up to 1·5 kbar. The Putirka *et al.* (2003) thermobarometer has a much larger average residual of 2·3 kbar.

Pressure of the low-Mg# rim analysis is reduced to 0·7–1·8 kbar, in line with the 1–2 kbar (i.e. 3–6 km) predicted using OPAM boundary barometry. The bulk of clinopyroxene analyses, however record pressures of crystallization greater than the OPAM estimates, with a maximum range of 2–5·4 kbar, which corresponds to a depth range of 8–20 km. Comparison with a 25 km crustal

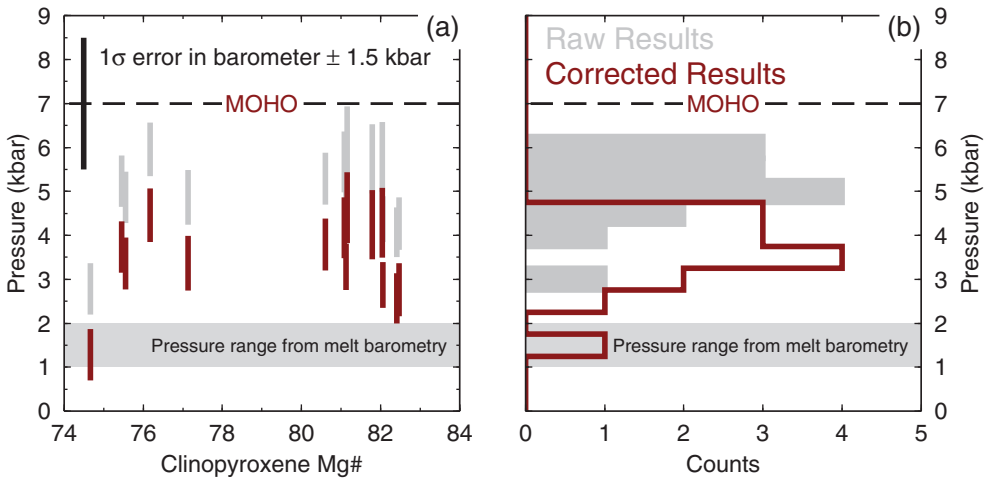

Fig. 15. (a) Crystallization pressures for Laki clinopyroxenes. Pressures were calculated using the cpx–melt barometer of Putirka (2008) on carefully matched equilibrium clinopyroxene–melt pairs. The method employed is described fully in the text. The 1–2 kbar range of carrier liquid equilibration is shown in pale grey. Raw barometry results are shown as pale lines. Results corrected for the systematic error in the barometer are shown as dark lines. Systematic error was determined by application of the Putirka (2008) barometer to experimental data in the 2–5 kbar range. Apart from a crystal rim that equilibrated at 0·7–1·8 kbar, clinopyroxene cores record crystallization pressures of 2–5·4 kbar. Comparison with a Moho depth of ~25 km (Darbyshire *et al.*, 2000) indicates that most crystallization of phenocrysts in the Laki system took place in the mid-crust. (b) Summary histogram using the same shading as in (a).

thickness from Darbyshire *et al.* (2000) implies that the bulk of crystallization in the Laki magma took place within the mid-crust. This depth range is comparable with that reported for magma movement events in recent studies of seismicity associated with the 2010 Eyjafjallajökull eruption (Tarasewicz *et al.*, 2012). This indicates that mid-crustal processing of magma may be an important feature across the EVZ.

Magmatic mushes and mid-crustal crystallization

Clinopyroxene–melt thermobarometry indicates that crystallization of plagioclase mantles, olivine cores and clinopyroxene cores occurred within the mid-crust across a maximum pressure range of 2–5·4 kbar. Oscillatory zoning in plagioclase mantles indicates that numerous recharge events took place during storage in the mid-crust. Melt inclusion data and plagioclase core compositions show that a range of mantle melt compositions were supplied during these recharge events, rather than a primitive melt of constant composition.

Textural evidence indicates that crystal settling and formation of polymineralic mushes took place prior to macrocryst rim growth. EMPA analyses as well as BSE and CL imagery show that macrocryst rims wrap around numerous cores, with crystal boundaries inside glomerocrysts never reaching the more evolved compositions of the macrocryst rims in contact with the groundmass (Figs 7 and 8). Mush formation is therefore likely to have occurred in the mid-crust (2–5·4 kbar), with the mush disaggregating into clots prior to transport to shallower levels where rim crystallization occurred (shown schematically in Fig. 16). The formation of magmatic mushes at mid- to deep crustal levels along the rift zones of Iceland has previously been proposed by Hansen & Grönvold (2000). Melt barometry indicates that final equilibration of macrocryst rims and the carrier liquid took place at 1–2 kbar during potentially brief shallow storage en route towards the surface. The mush addition signature suggested by Passmore *et al.* (2012) on the basis of whole-rock geochemistry and crystal proportion systematics must have been generated at the same depth as, or shallower than, the depth of last carrier liquid–crystal rim equilibration recorded by melt barometry (1–2 kbar). The mush formation recorded by crystal textures and compositions must have occurred in a different, earlier phase of melt evolution, deeper in the crust.

Bindeman *et al.* (2006) proposed that 25–45% of the volume of the Laki magma may have been derived by bulk digestion of Pleistocene hyaloclastite prior to eruption. Those workers argued that this digestion is required to explain the low and homogeneous $\delta^{18}O$ of the Laki–Grímsvötn system of ~3·1‰. In this model the material added from the hyaloclastite to the magma is of identical composition to the magma apart from having a lower $\delta^{18}O$ signature as the result of interaction with low $\delta^{18}O$ meltwater during emplacement and palagonitization. This model, however, is difficult to reconcile with the trace element data presented here. Melt inclusion trace element data show evidence of mixing of initially heterogeneous compositions towards a mean value corresponding to the carrier liquid. The $\delta^{18}O$ data, in contrast, would imply

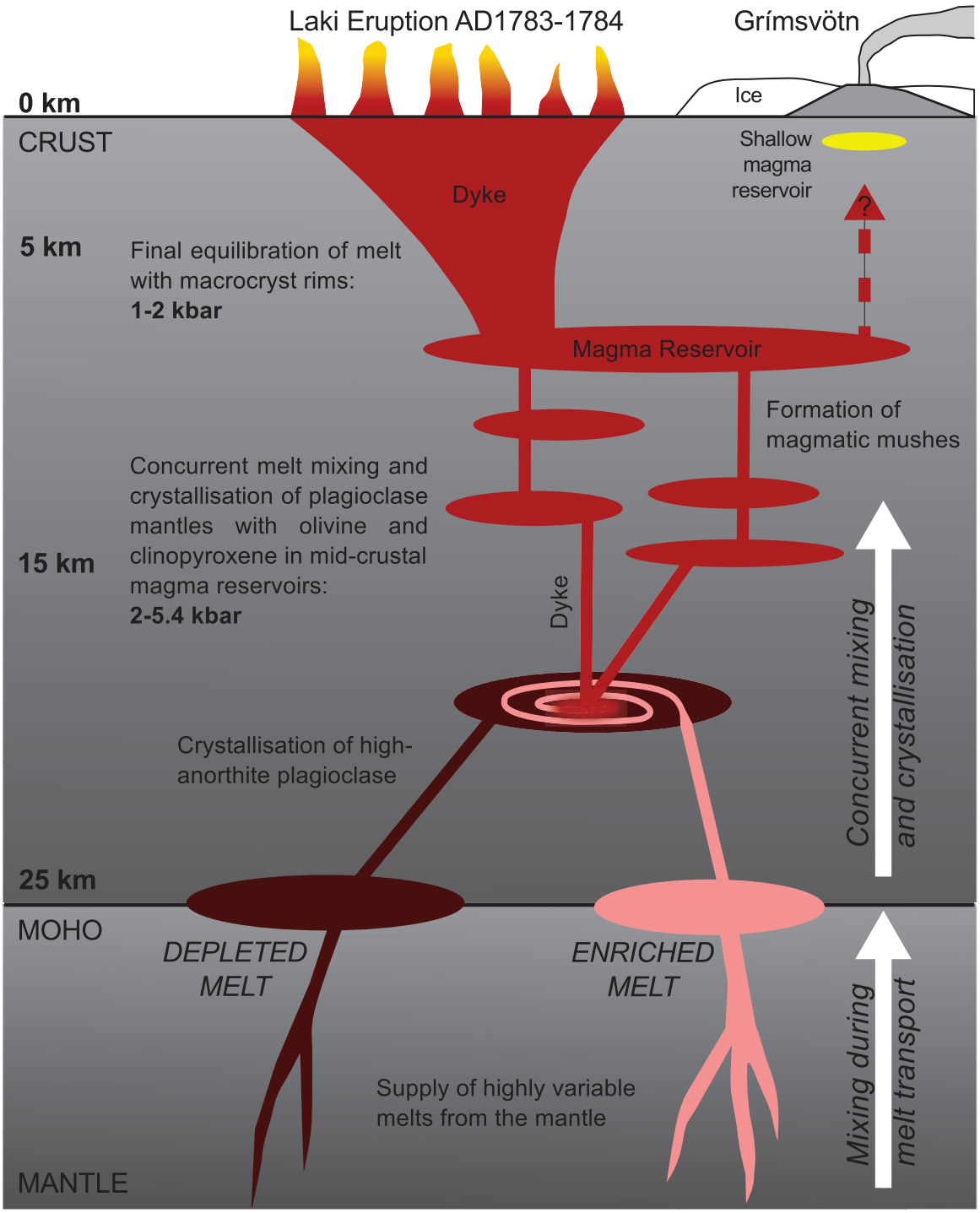

Fig. 16. Schematic illustration summarizing the record of deep processes in the Laki system and showing stylized plumbing system geometry. Olivine-hosted melt inclusions preserve a history of concurrent mixing and crystallization of melts of variable composition. Melts have undergone a significant amount of mixing prior to entrapment, indicating that mixing during melt transport has also occurred. High-anorthite plagioclase cores crystallized from highly depleted melts that are not preserved in the melt inclusion record. Plagioclase mantle oscillatory zonation patterns suggest that the crystallization occurred in melt of variable composition. This compositional variability may be attributed to mixing of variably fractionated melts, but may also be the result of supply of variable melts into the system. Clinopyroxene–melt barometry indicates that the bulk of olivine, plagioclase and clinopyroxene crystallization took place in mid-crustal magma reservoirs at 2–5·4 kbar. Formation of magmatic mushes at mid-crustal depths is inferred from crystal textures. These mushes were then disaggregated and transported in the carrier liquid as lone phenocrysts or as glomerocrysts to a region of shallow-crustal storage. Melt barometry constrains this depth of storage to ~1–2 kbar. Crystal rims grew at this depth, wrapping around macrocrysts and glomerocrysts. The mush addition signature identified by Passmore *et al.* (2012) must have been generated at the depth of last crystal–melt equilibration, or shallower. The compositional similarity between the erupted products of Laki and Grímsvötn may be the result of deep links in the plumbing system.

mixing towards an extreme light value rather than a mean value within the range suggested by the crystal compositions (the range of $\delta^{18}O$ in plagioclase and olivine macrocrysts is 2·2–5·2‰). The volume of material required to cause a shift in $\delta^{18}O$ to ~3·1‰ is very large (25–40%) and, as such it is difficult to envisage that it would not have an effect on the trace element content of the carrier liquid, which is not observed. We acknowledge that although our findings need not be incompatible with the model of Bindeman *et al.* (2006), it is possible that the low $\delta^{18}O$ of the Laki–Grímsvötn system may have other causes.

Crystallization at different levels in the crust strongly suggests that melt reservoirs are present at a range of depths in the EVZ crust. This is consistent with a 'stacked sills' model (e.g. Kelemen *et al.*, 1997; Maclennan *et al.*, 2001) of crustal accretion, as opposed to a 'gabbro glacier' model (e.g. Henstock *et al.*, 1993; Phipps Morgan & Chen, 1993), where crystallization occurs at shallow levels and crust is advected downwards. Information about crystallization depths cannot, however, provide information about the lateral transport history of the magma. All that can be constrained from the thermobarometry presented here is that magma storage has been recorded at 1–2 kbar and 2–5·4 kbar intervals, which may have been transient in the case of 1–2 kbar storage. Whether this storage was under Grímsvötn (Sigurdsson & Sparks, 1978) or dispersed over the fissure swarm (Gudmundsson, 1995) is unresolvable with our observations. Thordarson & Self (1993) have strongly argued against a lateral flow model for Laki on the basis of progressive opening of fissures towards Grímsvötn and the lack of evidence of large-scale drainage of magma and deflation at the central volcano.

CONCLUSIONS

The Laki eruption is striking because of its exceptional size and high eruption rates. However, detailed study of crystal–melt relationships indicates that magmatic evolution in the Laki system was governed by the same processes as smaller eruptions elsewhere in Iceland. Both melt inclusions and macrocrysts show evidence for a supply of diverse mantle melts to the base of the plumbing system. However, melt inclusions in forsteritic olivine do not record the full range of melt compositions generated by mantle melting. High-anorthite plagioclase macrocryst cores crystallized from high-Ca/Na, depleted melts, which are not represented in the melt inclusion population. It is not possible to resolve whether the cores have been incorporated from the walls of the plumbing system or represent an accumulated population mixed into parental carrier liquid prior to olivine-hosted melt inclusion entrapment. Depleted melts are likely to have been derived from shallow melting of refractory mantle. As a result of their high Ca/Na, depleted melts are expected to saturate in plagioclase much earlier during low-pressure fractional crystallization than enriched melts. Melt mixing, density sorting and/or diffusive overprinting of crystal compositions may prevent other magmatic components from carrying a record of such depleted melts. Despite the rest of the macrocryst load being largely out of equilibrium with the host lava, it is possible to relate it to the carrier liquid using fractional crystallization models. Oscillatory zoned plagioclase mantles record growth from variable melt compositions resulting from repeated recharge and crystallization events. Given the wide range of La/Yb in olivine-hosted melt inclusions in equilibrium with plagioclase mantles, it is therefore surprising that models using single liquid lines of descent are capable of reproducing observed crystal compositions as well as they do.

Reduction of melt inclusion trace element variability towards the flow mean with decreasing host olivine forsterite indicates that variable mantle melts were well mixed prior to eruption. Mixing rates calculated for Laki are similar to those previously calculated in the NVZ, Western Volcanic Zone and Reykjanes Peninsula. This is despite the higher magma supply rate in the EVZ and the large size of Laki in contrast to previously studied eruptions. Different thermobarometric techniques are capable of extracting a history of polybaric magmatic evolution (Fig. 16). Clinopyroxene–melt barometry indicates that most eutectic crystallization of macrocryst phases took place within the mid-crust at pressures of 2–5·4 kbar, in the depth range 8–20 km. The carrier liquid composition records final crystal–melt equilibration and macrocryst rim growth at a depth of 3–6 km in the shallow crust immediately before eruption. Crystal textures indicate that polymineralic magmatic mushes developed during mid-crustal storage and partially disaggregated upon transport of material to shallower levels. Polybaric crystallization in the Laki system provides further support for a stacked sill model of plumbing system geometry in Iceland where melt evolves and is stored at a range of depths, but much of the crystallization occurs in the mid- to lower crust.

ACKNOWLEDGEMENTS

We would like to thank Dr Stephen Elphick for his help with the 1 atm gas-mixing furnaces, and David Steele for assistance with EMPA at the University of Edinburgh. We would like to thank Martin Walker for his help with sample preparation and SEM, Dr Chiara Petrone for her help with EMPA, and Dr Olivier Namur for discussions regarding plagioclase–melt equilibrium and for sharing experimental datasets at the University of Cambridge. We would like to thank the staff at the NERC Ion Microprobe Facility at Edinburgh for their assistance with data collection and analysis. We would like to thank Oliver Shorttle, Margaret Hartley, Marie Edmonds, Sally

Gibson and Madeline Humphreys for helpful discussions during the preparation of this paper. We would also like to thank Lotte Larsen, Philipp Ruprecht and Leonid Danyushevsky for their detailed reviews, which greatly helped to improve the clarity of our arguments, and Marjorie Wilson for her editorial handling of this paper.

FUNDING

This work was supported by a Natural Environment Research Council studentship to D.A.N. (NE/1528277/1), a Natural Environment Research Council studentship to E.P. (NER/S/A/2004/12727) and a Natural Environment Research Council Ion Microprobe Facility award.

SUPPLEMENTARY DATA

Supplementary data for this paper are available at *Journal of Petrology* online.

REFERENCES

Abràmoff, M. D., Magalhaes, P. J. & Ram, S. J. (2004). Image processing with ImageJ. *Biophotonics International* **111**, 36–43.

Armienti, P. (2008). Description of igneous rock textures: crystal size distribution tools. In: Putirka, K. D. & Tepley, F. J., III (eds) *Minerals, Inclusions and Volcanic Processes. Mineralogical Society of America and Geochemical Society, Reviews in Mineralogy and Geochemistry* **69**, 623–649.

Bédard, J. H. (2005). Partitioning coefficients between olivine and silicate melts. *Lithos* **83**, 394–419.

Bender, J. F., Hodges, F. N. & Bence, A. E. (1978). Petrogenesis of basalts from the project FAMOUS area: experimental study from 0 to 15 kbars. *Earth and Planetary Science Letters* **41**, 277–302.

Bindeman, I. N. & Davis, A. M. (2000). Trace element partitioning between plagioclase and melt: investigation of dopant influence on partition behavior. *Geochimica et Cosmochimica Acta* **64**, 2863–2878.

Bindeman, I. N., Sigmarsson, O. & Eiler, J. (2006). Time constraints on the origin of large volume basalts derived from O-isotope and trace element mineral zoning and U-series disequilibria in the Laki and Grímsvötn volcanic system. *Earth and Planetary Science Letters* **245**, 245–259.

Breddam, K. (2002). Kistufell: Primitive melt from the Iceland mantle plume. *Journal of Petrology* **43**, 345–373.

Costa, F. & Morgan, D. (2010). Time constraints from chemical equilibration in magmatic crystals. In: Dosseto, A., Turner, S. P. & Van Orman, J. A. (eds) *Timescales of Magmatic Processes: From Core to Atmosphere*, 1st edn. Blackwell Publishing Ltd., pp. 125–159.

Cox, K. G., Bell, J. D. & Pankhurst, R. J. (1979). *The Interpretation of Igneous Rocks*. London: Chapman & Hall.

Danyushevsky, L. (2001). The effect of small amounts of H_2O on crystallisation of mid-ocean ridge and backarc basin magmas. *Journal of Volcanology and Geothermal Research* **110**, 265–280.

Danyushevsky, L. V. & Plechov, P. (2011). Petrolog3: Integrated software for modeling crystallization processes. *Geochemistry, Geophysics, Geosystems* **12**, Q07021.

Danyushevsky, L. V., McNeill, A. W. & Sobolev, A. V. (2002). Experimental and petrological studies of melt inclusions in phenocrysts from mantle-derived magmas: An overview of techniques, advantages and complications. *Chemical Geology* **183**, 5–24.

Danyushevsky, L. V., Perfit, M. R., Eggins, S. M. & Falloon, T. J. (2003). Crustal origin for coupled 'ultra-depleted' and 'plagioclase' signatures in MORB olivine-hosted melt inclusions: evidence from the Siqueiros Transform Fault, East Pacific Rise. *Contributions to Mineralogy and Petrology* **144**, 619–637.

Danyushevsky, L. V., Leslie, R. A. J., Crawford, A. J. & Durance, P. (2004). Melt inclusions in primitive olivine phenocrysts: The role of localized reaction processes in the origin of anomalous compositions. *Journal of Petrology* **45**, 2531–2553.

Darbyshire, F. A., White, R. S. & Priestley, K. F. (2000). Structure of the crust and uppermost mantle of Iceland from a combined seismic and gravity study. *Earth and Planetary Science Letters* **181**, 409–428.

Davidson, J. P., Morgan, D. J., Charlier, B. L. A., Harlou, R. & Hora, J. R. (2007). Microsampling and isotopic analysis of igneous rocks: implications for the study of magmatic systems. *Annual Review of Earth and Planetary Sciences* **35**, 273–311.

Elthon, D. & Casey, J. F. (1985). The very depleted nature of certain primary mid-ocean ridge basalts. *Geochimica et Cosmochima Acta* **49**, 289–298.

Feig, S. T., Koepke, J. & Snow, J. E. (2006). Effect of water on tholeiitic basalt phase equilibria: an experimental study under oxidizing conditions. *Contributions to Mineralogy and Petrology* **152**, 611–638.

Feig, S. T., Koepke, J. & Snow, J. E. (2010). Effect of oxygen fugacity and water on phase equilibria of a hydrous tholeiitic basalt. *Contributions to Mineralogy and Petrology* **160**, 551–568.

Gast, P. (1968). Trace element fractionation and the origin of tholeiitic and alkaline magma types. *Geochimica et Cosmochimica Acta* **32**, 1057–1086.

Geirsson, H., Árnadóttir, T., Völkson, C., Jiang, W., Sturkell, E., Villemin, T., Einarsson, P., Sigmundsson, F. & Stefánsson, R. (2006). Current plate movements across the Mid-Atlantic Ridge determined from 5 years of continuous GPS measurements in Iceland. *Journal of Geophysical Research* **111**, 1–18.

Ginibre, C., Kronz, A. & Wörner, G. (2002*a*). High-resolution quantitative imaging of plagioclase composition using accumulated backscattered electron images: new constraints on oscillatory zoning. *Contributions to Mineralogy and Petrology* **142**, 436–448.

Ginibre, C., Wörner, G. & Kronz, A. (2002*b*). Minor- and trace-element zoning in plagioclase: implications for magma chamber processes at Parinacota volcano, northern Chile. *Contributions to Mineralogy and Petrology* **143**, 300–315.

Grove, T. L. (1993). Corrections to expressions for calculating mineral components in 'Origin of calc-alkaline series lavas at Medicine Lake volcano by fractionation, assimilation and mixing' and 'Experimental petrology of normal MORB near the Kane Fracture Zone: 22–25°N, Mid-Atlantic Ridge'. *Contributions to Mineralogy and Petrology* **114**, 422–424.

Grove, T. L., Baker, M. B. & Kinzler, R. J. (1984). Coupled CaAl–NaSi diffusion in plagioclase feldspar: Experiments and applications to cooling rate speedometry of many metamorphic environments. *Geochimica et Cosmochimica Acta* **48**, 2113–2121.

Grove, T. L., Kinzler, R. J. & Bryan, W. B. (1992). Fractionation of mid-ocean ridge basalt (MORB). In: Phipps-Morgan, J., Blackman, D. K. & Sinton, J. M. (eds) *Mantle Flow and Melt Generation at Mid-ocean Ridges*. Washington, DC: American Geophysical Union, **71**, 281–310.

Gudmundsson, A. (1995). Infrastructure and mechanics of volcanic systems in Iceland. *Journal of Volcanology and Geothermal Research* **64**, 1–22.

Guilbaud, M.-N., Blake, S., Thordarson, T. & Self, S. (2007). Role of syn-eruptive cooling and degassing on textures of lavas from the

AD 1783–1784 Laki eruption, south Iceland. *Journal of Petrology* **48**, 1265–1294.

Gurenko, A. A. & Chaussidon, M. (1995). Enriched and depleted primitive melts included in olivine from Icelandic tholeiites—Origin by melting of a single mantle column. *Geochimica et Cosmochimica Acta* **59**, 2905–2917.

Gurenko, A. A. & Chaussidon, M. (1997). Boron concentrations and isotopic composition of the Icelandic mantle: evidence from glass inclusions in olivine. *Chemical Geology* **135**, 21–34.

Gurenko, A. A. & Chaussidon, M. (2002). Oxygen isotope variations in primitive tholeiites of Iceland: evidence from a SIMS study of glass inclusions, olivine phenocrysts and pillow rim glasses. *Earth and Planetary Science Letters* **205**, 63–79.

Gurenko, A. A. & Sobolev, A. V. (2006). Crust–primitive magma interaction beneath neovolcanic rift zone of Iceland recorded in gabbro xenoliths from Midfell, SW Iceland. *Contributions to Mineralogy and Petrology* **151**, 495–520.

Halldorsson, S. A., Oskarsson, N., Grönvold, K., Sigurdson, G., Sverrisdottir, G. & Steinthorsson, S. (2008). Isotopic heterogeneity of the Thjórsá lava—Implications for mantle sources and crustal processes within the Eastern Rift Zone, Iceland. *Chemical Geology* **255**, 305–316.

Hammer, J. E. & Rutherford, M. J. (2002). An experimental study of the kinetics of decompression-induced crystallization in silicic melt. *Journal of Geophysical Research* **107**, 2021, doi: 10.1029/2001B000281.

Hansen, H. & Grönvold, K. (2000). Plagioclase ultraphyric basalts in Iceland: The mush of the rift. *Journal of Volcanology and Geothermal Research* **98**, 1–32.

Harker, A. (1896). On certain granophyres, modified by the incorporation of gabbro-fragments, in Strath Skye. *Quarterly Journal of the Geological Society of London* **52**, 320–330.

Henstock, T. J., Woods, A. W. & White, R. S. (1993). The accretion of oceanic crust by episodic sill intrusion. *Journal of Geophysical Research* **98**, 4143–4161.

Higgins, M. D. (2000). Measurement of crystal size distributions. *American Mineralogist* **85**, 1105–1116.

Hill, E., Blundy, J. D. & Wood, B. J. (2010). Clinopyroxene–melt trace element partitioning and the development of a predictive model for HFSE and Sc. *Contributions to Mineralogy and Petrology* **161**, 423–438.

Hjaltadóttir, S., Vogfjörð, K. S. & Slunga, R. (2009). *Seismic signs of magma pathways through the crust in the Eyjafjallajökull volcano, south Iceland, Report VI 2009-13.* Reykjavik: Icelandic Meteorology Office.

Holness, M. B., Anderson, A. T., Martin, V. M., Maclennan, J., Passmore, E. & Schwindinger, K. (2007). Textures in partially solidified crystalline nodules: a window into the pore structure of slowly cooled mafic intrusions. *Journal of Petrology* **48**, 1243–1264.

Humphreys, M. C. S. (2009). Chemical evolution of intercumulus liquid, as recorded in plagioclase overgrowth rims from the Skaergaard intrusion. *Journal of Petrology* **50**, 127–145.

Jakobsson, S. P. (1979). Petrology of Recent basalts of the Eastern Volcanic Zone, Iceland. *Acta Naturalia Islandica* **26**, 18.

Jochum, K. P., Weis, U., Stoll, B., Kuzmin, D., Yang, Q., Raczek, I., Jacob, D. E., Stracke, A., Birbaum, K., Frick, D. A., Günther, D. & Enzweiler, J. (2011). Determination of reference values for NIST SRM 610–617 glasses following ISO guidelines. *Geostandards and Geoanalytical Research* **35**, 397–429.

Jurewicz, A. J. G. & Watson, E. B. (1988). Cations in olivine, Part 2: Diffusion in olivine xenocrysts, with applications to petrology and mineral physics. *Contributions to Mineralogy and Petrology* **99**, 186–201.

Kelemen, P. B., Hirth, G., Shimizu, N., Spiegelman, M. & Dick, H. J. B. (1997). A review of melt migration processes in the asthenospheric mantle beneath oceanic spreading centers. *Philosophical Transactions of the Royal Society of London, Series A* **355**, 283–318.

LaFemina, P. C., Dixon, T. H., Malservisi, R., Árnadóttir, T., Sturkell, E., Sigmundsson, F. & Einarsson, P. (2005). Geodetic GPS measurements in south Iceland: Strain accumulation and partitioning in a propagating ridge system. *Journal of Geophysical Research B: Solid Earth* **110**, 1–21.

Lange, R. A. (1997). A revised model for the density and thermal expansivity extension to crustal magmatic temperatures. *Contributions to Mineralogy and Petrology* **130**, 1–11.

Lange, R. L. & Carmichael, I. S. (1990). Thermodynamic properties of silicate liquids with emphasis on density, thermal expansion and compressibility. In: Nicholls, J. & Russell, J. K. (eds) *Modern Methods of Igneous Petrology: Understanding Magmatic Processes. Mineralogical Society of America, Reviews in Mineralogy* **24**, 25–64.

Larsen, G. (2000). Holocene eruptions within the Katla volcanic system, south Iceland: characteristics and environmental impact. *Jökull* **49**, 1–28.

LaTourrette, T. & Wasserburg, G. J. (1998). Mg diffusion in anorthite: implications for the formation of early solar system planetesimals. *Earth and Planetary Science Letters* **158**, 91–108.

Maclennan, J. (2008*a*). Concurrent mixing and cooling of melts under Iceland. *Journal of Petrology* **49**, 1931–1953.

Maclennan, J. (2008*b*). Lead isotope variability in olivine-hosted melt inclusions from Iceland. *Geochimica et Cosmochimica Acta* **72**, 4159–4176.

Maclennan, J., McKenzie, D., Grönvold, K. & Slater, L. (2001). Crustal accretion under Northern Iceland. *Earth and Planetary Science Letters* **191**, 295–310.

Maclennan, J., McKenzie, D., Grönvold, K., Shimizu, N., Eiler, J. M. & Kitchen, N. (2003*a*). Melt mixing and crystallization under Theistareykir, northeast Iceland. *Geochemistry, Geophysics, Geosystems* **4**, 8624.

Maclennan, J., McKenzie, D., Hilton, F., Grönvold, K. & Shimizu, N. (2003*b*). Geochemical variability in a single flow from northern Iceland. *Journal of Geophysical Research* **108**, 1–21.

Marks, N., Schiffman, P. & Zierenberg, R. (2011). High-grade contact metamorphism in the Reykjanes geothermal system: implications for fluid–rock interactions at mid-oceanic ridge spreading centres. *Geochemistry, Geophysics, Geosystems* **12**, Q08007.

Marsh, B. D. (1988). Crystal size distribution (CSD) in rocks and the kinetics and dynamics of crystallization. 1. Theory. *Contributions to Mineralogy and Petrology* **99**, 277–291.

Métrich, N., Sigurdsson, H., Meyer, P. S. & Devine, J. D. (1991). The 1783 Lakagígar eruption in Iceland: geochemistry, CO_2 and sulfur degassing. *Contributions to Mineralogy and Petrology* **107**, 435–447.

Morgan, D. J. & Jerram, D. A. (2006). On estimating crystal shape for crystal size distribution analysis. *Journal of Volcanology and Geothermal Research* **154**, 1–7.

Moune, S., Sigmarsson, O., Schiano, P., Thordarson, T. & Keiding, J. K. (2012). Melt inclusion constraints on the magma source of Eyjafjallajökull 2010 flank eruption. *Journal of Geophysical Research* **117**, 1–13.

Nakamura, Y. (1973). Origin of sector-zoning of igneous clinopyroxenes. *American Mineralogist* **58**, 986–990.

Namur, O., Charlier, B., Toplis, M. J. & Vander Auwera, J. (2011). Prediction of plagioclase–melt equilibria in anhydrous silicate melts at 1-atm. *Contributions to Mineralogy and Petrology* **163**, 133–150.

Nichols, A., Carroll, M. & Hoskuldsson, Á. (2002). Is the Iceland hot spot also wet? Evidence from the water contents of undegassed submarine and subglacial pillow basalts. *Earth and Planetary Science Letters* **202**, 77–87.

Óskarsson, N., Helgason, Ö. & Steinthórsson, S. (1994). Oxidation state of iron in mantle-derived magmas of the Icelandic rift zone. *Hyperfine Interactions* **91**, 733–737.

Panjasawatwong, Y., Danyushevsky, L. V., Crawford, A. J. & Harris, K. L. (1995). An experimental study of the effects of melt composition on plagioclase–melt equilibria at 5 and 10 kbar: implications for the origin of magmatic high-An plagioclase. *Contributions to Mineralogy and Petrology* **118**, 420–432.

Passmore, E., Maclennan, J., Fitton, G. & Thordarson, T. (2012). Mush disaggregation in basaltic magma reservoirs: Evidence from the AD 1783 Laki Eruption. *Journal of Petrology* **53**, 2593–2623.

Phipps Morgan, J. & Chen, Y. (1993). The genesis of oceanic crust, magma injection, hydrothermal circulation and crustal flow. *Journal of Geophysical Research* **98**, 6283–6297.

Putirka, K. D. (1999). Clinopyroxene + liquid equilibria to 100 kbar and 2450 K. *Contributions to Mineralogy and Petrology* **135**, 151–163.

Putirka, K. D. (2005). Igneous thermometers and barometers based on plagioclase + liquid equilibria: Tests of some existing models and new calibrations. *American Mineralogist* **90**, 336–346.

Putirka, K. D. (2008). Thermometers and barometers for volcanic systems. In: Putirka, K. D. & Tepley, F. J., III (eds) *Minerals, Inclusions and Volcanic Processes. Mineralogical Society of America and Geochemical Society, Reviews in Mineralogy and Geochemistry* **69**, 61–120.

Putirka, K. D., Johnson, M., Kinzler, R., Longhi, J. & Walker, D. (1996). Thermobarometry of mafic igneous rocks based on clinopyroxene–liquid equilibria, 0–30 kbar. *Contributions to Mineralogy and Petrology* **123**, 92–108.

Putirka, K. D., Mikaelian, H., Ryerson, F. J. & Shaw, H. (2003). New clinopyroxene–liquid thermobarometers for mafic, evolved, and volatile-bearing lava compositions, with applications to lavas from Tibet and the Snake River Plain, Idaho. *American Mineralogist* **88**, 1542–1554.

Reed, S. J. B. (2005). *Electron Microprobe Analysis and Scanning Electron Microscopy in Geology*. Cambridge: Cambridge University Press.

Roeder, P. L. & Emslie, R. F. (1970). Olivine–liquid equilibrium. *Contributions to Mineralogy and Petrology* **29**, 275–289.

Ruprecht, P., Bergantz, G. W. & Dufek, J. (2008). Modeling of gas-driven magmatic overturn: Tracking of phenocryst dispersal and gathering during magma mixing. *Geochemistry, Geophysics, Geosystems* **9**, Q07017.

Saal, A., Hart, S., Shimizu, N., Hauri, E. & Layne, G. (1998). Pb isotopic variability in melt inclusions from oceanic island basalts, Polynesia. *Science* **282**, 1481–1484.

Schwindinger, K. (1999). Particle dynamics and aggregation of crystals in a magma reservoir with application to Kilauea Iki olivines. *Journal of Volcanology and Geothermal Research* **88**, 209–238.

Shorttle, O. & Maclennan, J. (2011). Compositional trends of Icelandic basalts: Implications for short-lengthscale lithological heterogeneity in mantle plumes. *Geochemistry, Geophysics, Geosystems* **12**, Q11008.

Sigmarsson, O. & Steinthorsson, S. (2007). Origin of Icelandic basalts: A review of their petrology and geochemistry. *Journal of Geodynamics* **43**, 87–100.

Sigmarsson, O., Condomines, M., Grönvold, K. & Thordarson, T. (1991). Extreme magma homogeneity in the 1783–84 Lakagigar eruption: origin of a large volume of evolved basalt in Iceland. *Geophysical Research Letters* **18**, 2229–2232.

Sigmundsson, F., Hreinsdóttir, S., Hooper, A., Arnadóttir, T., Pedersen, R., Roberts, M. J., Oskarsson, N., Auriac, A., Decriem, J., Einarsson, P., Geirsson, H., Hensch, M., Ofeigsson, B. G., Sturkell, E., Sveinbjörnsson, H. & Feigl, K. L. (2010). Intrusion triggering of the 2010 Eyjafjallajökull explosive eruption. *Nature* **468**, 426–30.

Sigurdsson, H. & Sparks, R. (1978). Lateral magma flow within rifted Icelandic crust. *Nature* **274**, 126–130.

Sisson, T. (1993). Experimental investigations of the role of H_2O in calc-alkaline differentiation and subduction zone magmatism. *Contributions to Mineralogy and Petrology* **113**, 143–166.

Skinner, E. M. W. & Clement, C. R. (1979). Mineralogical classification of southern African kimberlites. In: Boyd, F. R. & Meyer, H. O. A. (eds) *Kimberlites, Diatremes, and Diamonds: Their Geology, Petrology, and Geochemistry*. Washington, DC: American Geophysical Union, pp. 129–139.

Slater, L., McKenzie, D., Grönvold, K. & Shimizu, N. (2001). Melt generation and movement beneath Theistareykir, NE Iceland. *Journal of Petrology* **42**, 321–354.

Smyth, J. R. & McCormick, T. C. (1995). Crystallographic data for minerals. In: Ahrens, T. J. (ed.) *Mineral Physics and Crystallography: A Handbook of Physical Constants*. Washington, DC: American Geophysical Union, pp. 1–17.

Sobolev, A. V. & Shimizu, N. (1993). Ultra-depleted primary melt included in an olivine from the Mid-Atlantic Ridge. *Nature* **363**, 151–154.

Spandler, C. & O'Neill, H. S. C. (2010). Diffusion and partition coefficients of minor and trace elements in San Carlos olivine at 1300°C with some geochemical implications. *Contributions to Mineralogy and Petrology* **159**, 791–818.

Steinthorsson, S., Óskarsson, N. & Sigvaldason, G. E. (1985). Origin of alkali basalts in Iceland: a plate tectonic model. *Journal of Geophysical Research* **90**, 10027–10042.

Takahashi, E. & Kushiro, I. (1983). Melting of a dry peridotite at high pressures and basalt magma genesis. *American Mineralogist* **68**, 859–879.

Tarasewicz, J., Brandsdóttir, B., White, R. S., Hensch, M. & Thorbjarnardóttir, B. (2012). Using microearthquakes to track repeated magma intrusions beneath the Eyjafjallajökull stratovolcano, Iceland. *Journal of Geophysical Research* **117**, 1–13.

Thomson, A. & Maclennan, J. (2013). The distribution of olivine compositions in Icelandic basalts and picrites. *Journal of Petrology* **54**, 745–768.

Thordarson, T. & Höskuldsson, Á. (2008). Postglacial volcanism in Iceland. *Jökull* **58**, 197–228.

Thordarson, T. & Larsen, G. (2007). Volcanism in Iceland in historical time: Volcano types, eruption styles and eruptive history. *Journal of Geodynamics* **43**, 118–152.

Thordarson, T. & Self, S. (1993). The Laki (Skaftár Fires) and Grímsvötn eruptions in 1783–1785. *Bulletin of Volcanology* **55**, 233–263.

Thordarson, T., Self, S., Oskarsson, N. & Hulsebosch, T. (1996). Sulfur, chlorine, and fluorine degassing and atmospheric loading by the 1783–1784 AD Laki (Skaftár Fires) eruption in Iceland. *Bulletin of Volcanology* **58**, 205–225.

Toothill, J., Williams, C. A., MacDonald, R., Turner, S. P., Rogers, N. W., Hawkesworth, C. J., Jerram, D. A., Ottley, C. J. & Tindle, A. G. (2006). A complex petrogenesis for an arc magmatic suite, St Kitts, Lesser Antilles. *Journal of Petrology* **48**, 3–42.

Toplis, M. J. & Carroll, M. R. (1995). An experimental study of the influence of oxygen fugacity on Fe–Ti oxide stability, phase relations, and mineral–melt equilibria in ferro-basaltic systems. *Journal of Petrology* **36**, 1137–1170.

Tormey, D. R., Grove, T. L. & Bryan, W. B. (1987). Experimental petrology of normal MORB near the Kane Fracture Zone: 20–25°N, Mid-Atlantic Ridge. *Contributions to Mineralogy and Petrology* **96**, 121–139.

Villiger, S., Müntener, O. & Ulmer, P. (2007). Crystallization pressures of mid-ocean ridge basalts derived from major element variations of glasses from equilibrium and fractional crystallization

experiments. *Journal of Geophysical Research B: Solid Earth* **112**, B01202.

Winpenny, B. & Maclennan, J. (2011). A partial record of mixing of mantle melts preserved in Icelandic phenocrysts. *Journal of Petrology* **52**, 1791–1812.

Wood, B. J. & Blundy, J. D. (1997). A predictive model for rare earth element partitioning between clinopyroxene and anhydrous silicate melt. *Contributions to Mineralogy and Petrology* **129**, 166–181.

Yang, H.-J., Kinzler, R. J. & Grove, T. L. (1996). Experiments and models of anhydrous, basaltic olivine–plagioclase–augite saturated melts from 0·001 to 10 kbar. *Contributions to Mineralogy and Petrology* **124**, 1–18.

Yoder, H. S. & Tilley, C. E. (1962). Origin of basalt magmas: an experimental study of natural and synthetic rock systems. *Journal of Petrology* **3**, 342–532.

Zhang, Y. (2010). Diffusion in minerals and melts: theoretical background. In: Zhang, Y. & Cherniak, D. J. (eds) *Diffusion in Minerals and Melts. Mineralogical Society of America and Geochemical Society, Reviews in Mineralogy and Geochemistry* **72**, 5–59.